NTNU – Trondheim
Norwegian University of
Science and Technology

Implementation and Testing of Numerical Models for Evolution of Microchemistry and Microstructure During Back-Annealing of Aluminium Alloys

Jørgen Tandberg Iversen

Materials Science and Engineering
Submission date: June 2014
Supervisor: Knut Marthinsen, IMTE
Co-supervisor: Jesper Friis, Sintef

Norwegian University of Science and Technology
Department of Materials Science and Engineering

Acknowledgements

First and foremost i would like to thank my supervisor Professor Knut Marthinsen for valuable advice and guidance during my work on this thesis. I would also like to thank my co-supervisor Jesper Friis at Sintef for providing good advice regarding how to implement the precipitation model, and how to couple it with Alsoft.

Finally i would like to thank my good friends Shuang Li, Mads Christensen and Guro Heintz for helping me keep the morale up during the many long days spent working on this thesis.

Abstract

Precipal and Alsoft are two separate models for simulating the effects of back-annealing on microchemistry and microstructure, respectively, in AA3xxx-type aluminium alloys (i.e Mn containing alloys). The precipitation model simulates the precipitation and growth of dispersoids, growth of constituents, and the resulting change in the solid solution concentration. Alsoft is a physical softening model which combines the effects of recovery and recrystallization.

Precipal was originally implemented in Fortran 77, while the softening model, Alsoft, is implemented in Python. It would be beneficial for both the precipitation and softening model to be coupled with each other, as both models provide parameters and state variables that are given as input parameters in the other model (e.g information about the precipitates from Precipal can be used to calculate the Zener-drag, currently given as an external input parameter in Alsoft).

In order to facilitate this coupling the precipitation model is reimplemented in Python. This model is then validated against the old implementation, and a parameter sensitivity study is performed to identify the most critical input parameters. The new implementation of the precipitation model is then coupled with the softening model and simulations has been performed and compared with experimental data.

Precipal consists of two different precipitation models: a physical model based on physical equations, and one phenomenological model which introduces a number of fitting parameters which are determined experimentally. The physical model was shown to have too fast and abrupt precipitation behavior compared with experimental results. The phenomenological model on the other hand was able to reproduce the experimental precipitation behavior at a given temperature, but failed to successfully predict the effect of different annealing temperatures.

The effects on the simulated recrystallization kinetics due to the coupling was found to be minimal, except when the precipitation halted recrystallization completely due to a large Zener-drag. The reason for this lacking effect it believed to be the assumption of site-saturation nucleation in Alsoft, which implies that the Zener-drag effect from concurrent precipitation on recrystallization nucleation is not modeled.

Sammendrag

Precipal og Alsoft er to separate modeller for å simulere effekten av tilbakegløding på henholdsvis mikrokjemi og mikrostruktur, i AA3XXX-type aluminiumslegeringer (dvs Mn holdige legeringer). Presipiteringsmodellen simulerer presipitering og vekst av dispersoider, vekst av primærpartikler, og den resulterende endringen i Mn konsentrasjonen i fast løsning. Alsoft er en fysikalsk mykningsmodell(softening model) som kombinerer effekten av gjenvinning og rekrystallisasjon.

Precipal ble opprinnelig implementert i Fortran 77, mens mykningsmodellen, Alsoft, er implementert i Python. Det vil være fordelaktig for begge modellene å bli koblet med hverandre, da begge modellene simulerer parametere som er gitt som input-parametere i den andre modellen (Informasjon om presipitater fra Precipal kan for eksempel brukes til å kalkulerer Zener-drag i Alsoft).

For å tilrettelegge for koblingen av de to modellene er presipiteringsmodellen reimplementert i Python. Denne modellen er så validert mot den orginale implementasjonen, og en følsomhetsanalyse er utørt for å identifisere de mest kritiske inputparametrene. Den nye implementeringen av presipiteringsmodellen blir så koblet med Alsoft, og simuleringer har blitt utført og sammenlignet med eksperimentelle data.

Precipal består av to separate presipiteringsmodeller: en fysisk modell baser på fysikalske ligniner, og en fenomenologisk modell som introduserer et antall tilpassningsparametere som må bestemmes eksperimentelt. Den fysikalske modellen viste seg å ha for rask og brå presipitering sammenlignet med eksperimentelle data, mens den fenomenologiske modellen kunne reprodusere eksperimentelle data for en gitt temperatur, men lykkes ikke med å forutsi effekten av forskjellige glødetemperaturer.

Effekten av koblingen på den simulerte rekrystallisasjonskinetikken var minimal, med unntak av når rekrystallisasjonen stoppet fullstendig pga et stort Zener-drag. årsaken til denne manglende effekten er antatt å komme fra antagelsen om site-saturation kimdanning i Alsoft, som medfører at Zener-drag effekten fra presipitering under gløding på rekrystallisasjonskimdanning ikke blir modelert.

Contents

1. Introduction

Manufacturing of aluminium alloy sheets involves a sequence of thermo mechanical treatment steps. During processing the material is first cast and homogenized, before being plastically deformed, usually by a number of rolling steps, first hot, then cold, followed by back-annealing, where the material is kept at an elevated temperature for an extended amount of time. This last step is used to get the desired mechanical properties by thermally activated changes to the microstructure, and it is of great industrial importance to be able to predict the effect of this heat treatment, and therefore this step is the focus of this thesis.

During annealing the deformed material will experience *recovery* (softening due to growth of sub-grains and annihilation of dislocations) and *recrystallization* (nucleation and growth of new dislocation free grains). These phenomena are modeled by the existing *Alsoft-Model* which is based on works by Marthinsen, Furu, and Vatne[1–3]. The model is an extension of the classical Johnson-Mehl-Avrami-Kolmogorov(JMAK) approach, and combines the effects of recovery and recrystallization.

During annealing of industrial aluminium alloys, precipitation of finely dispersed particles often occurs. This will have an effect on the recrystallization kinetics. Precipitation is not modeled in the original Alsoft-model. Currently its influence can only be handled through changes in external parameters, like the solute level and volume fraction and size of dispersoids. Precipitation is instead modeled in the separate *Precipal-model*, implemented at NTNU/Sintef by Friis[4, 5], based on a precipitation model developed in the PhD work of Lok[6].

In order to improve both the softening and precipitation model there is a need to couple the two separate models. Precipal was originally implemented in the Fortran programming language, while Alsoft recently has been implemented in Python. In this thesis Precipal is reimplemented in Python and the two models are coupled.

The new implementation(Python) of the precipitation model needs testing and validation before further use to new alloys and conditions. Testing/validation of the coupled softening(recovery and recrystallization) and precipitation model is desirable an needed in order to explore and demonstrate its potential, and to identify limitations and equally important deficiencies.

In this thesis the new implementation of Precipal is validated against the old Fortran implementation, and a sensitivity test is carried out in order to identify the most critical input parameters. Precipal is also validated against simulations preformed by Lok[6] (which are performed with another implementation of the same precipitation model). The effects of the coupling on the simulated recrystallization kinetics is explored, and compared with experimental data in an effort to improve and validate the predictive power of the coupled models.

2. Theory

In this chapter relevant theory for this work will be presented. First an explanation of thermomechanical processing used in aluminium sheet production, including the microchemical and microstructural changes in the material will be presented. After this the recovery and recrystallization model (Alsoft) and precipitation model (Precipal) will be introduced, including the principle of coupling these two models.

2.1. Thermomechanical processing

Thermomechanical processing (TMP) is widely used during production of commercial aluminium alloys in which deformation (rolling) and heat-treatment are alternated in a semi-continuous process. The different steps involved in this treatment are illustrated in Figure 2.1.

The first step after casting is pre-heating or homogenization, where the material is heated and held at temperatures up to 600 °C for up to several hours. During this step the *microstructure* (grain size, dislocation density and texture) is largely unchanged, while the *microchemistry* (solid-solution concentration of alloying elements, and the size and number density of particles) undergoes large changes. The solid solution concentration may be lowered as alloying elements will be dispersed as small particles inside the grains, or as larger particles at the grain boundaries[6, 7].

The next step in the process is rolling, where the material is plastically deformed by several rolling steps with gradually decreasing roll-gap. The rolling is typically performed at a temperature of about 350-450 °C (hot-rolling), followed by cold rolling at about 100 °C[6]. This changes the microstructure, as a high number of dislocations are introduced in the material, and thus results in a high degree of work hardening. The microchemistry may also be changed, as particles can precipitate during this step (depending on temperature)[6].

The final step in the process is annealing, where the material is held at an elevated temperature (300-450 °C) for some time (up to several hours). This step is necessary in order to get the desired combination of hardness and ductility. During this step both the microstructure and microchemistry undergoes substantial changes. The deformation microstructure(consisting of sub-grains and cell interior dislocations) will be removed by recrystallization where new, dislocation free grains are formed and more particles(dispersoids) can precipitate. It is this final step which is the focus of this thesis. The changes to the microstructure and microchemistry will be further explained in Section 2.2 and 2.3.

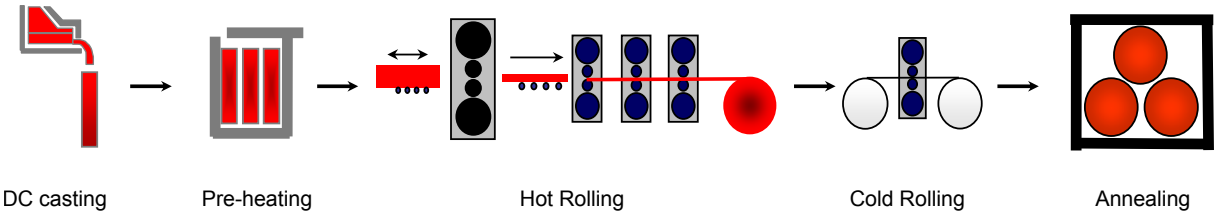

Figure 2.1.: Illustration of the different steps in a typical thermomechanical process [8].

2.2. Recovery and recrystallization of cold deformed material

During annealing there will be a combination of *recovery* and *recrystallization*. Recovery is characterized by growth of sub grains (grains with low angle grain boundaries) and annealing out (annihilation) of dislocations. Recrystallization consists of nucleation and growth of new dislocation free grains. Recovery and recrystallization are "competing" processes, and the material will experience a combination of these phenomena depending on the temperature, as illustrated in Figure 2.2. At low temperatures, recovery will be the dominating process, while at higher temperatures, recrystallization is most prominent. At medium temperatures the material will experience a combination, with initial recovery, followed by recrystallization. It is evident from Figure 2.2 that the hardness is reduced by both reactions, but the reduction is most pronounced during recrystallization.

Figure 2.3 schematicly shows the microstructure of an deformed aluminium alloy at increasing annealing times, with an annealing temperature corresponding with the "medium temperature case" in Figure 2.2, so that the material will experience recovery initially, followed by recrystallization. Immediately after rolling the grains are elongated and the dislocation density is high (Fig. 2.3a). When the annealing commences the dislocations will reorganize into sub grains and some will disappear due to annihilation (Fig. 2.3b). Further annealing will result in nucleation and growth of new dislocation free grains (Fig. 2.3c). This will normally continue until 100% of the material is recrystallized (Fig. 2.3d). If the annealing is continued the grains will normally continue to grow through normal grain growth (Fig. 2.3e), or possibly abnormal grain growth (Fig. 2.3f, also called secondary recrystallization).

Precipitation of particles will normally have an effect on the recrystallization kinetics, this is explained in the next section.

2.3. Precipitation of particles

There are two main categories of particles affecting the recrystallization kinetics in aluminium, *constituents* and *dispersoids* [6, 7]. The defining distinction is the size of the particles and when they are formed. Constituents are formed during casting and solidification, and are relatively large, with a radius of $\approx$ 1-50μm[11]. The dispersoids are mainly formed during processing and are substantially smaller, with a radius of only $\approx 0.1\mu$m [11]. In this section the effect of these two particle categories will be presented.

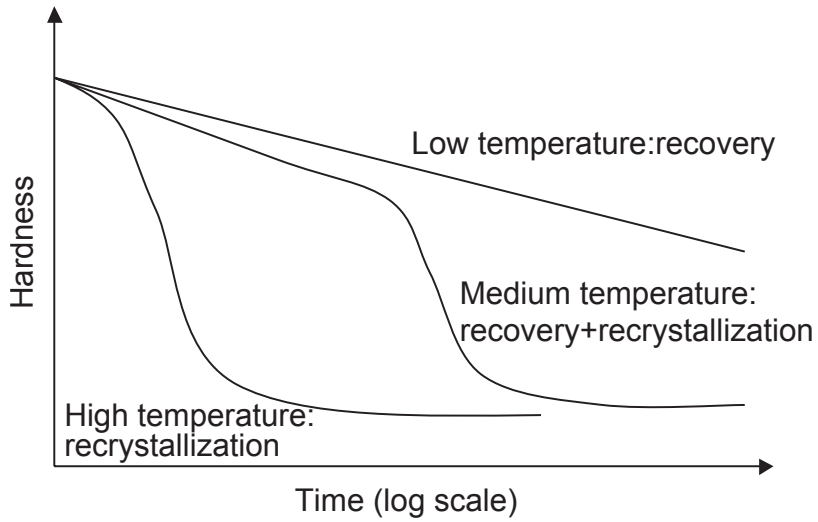

Figure 2.2.: Schematic of hardness vs time at different annealing temperatures after deformation. Based on figure from [9, p. 8].

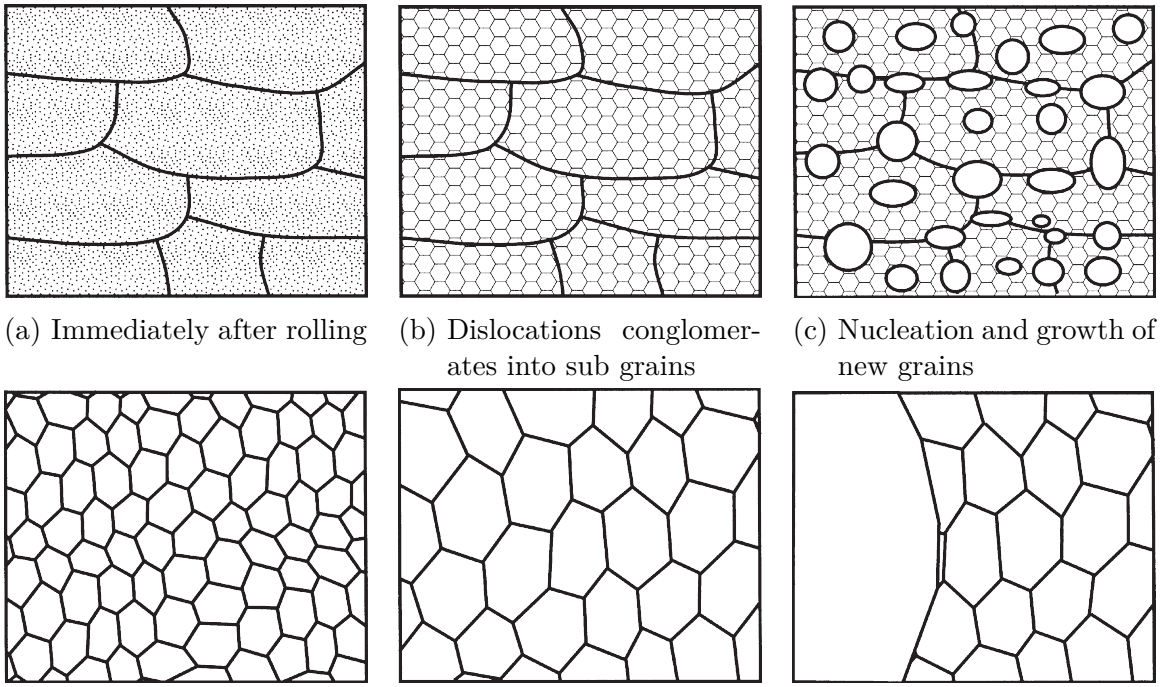

(a) Immediately after rolling

(b) Dislocations conglomerates into sub grains

(c) Nucleation and growth of new grains

(d) 100 % recrystallized

(e) Further grain growth

(f) Abnormal grain growth

Figure 2.3.: Illustration of the changes in the microstructure in a deformed aluminium alloy during back-annealing[10, s. 2].

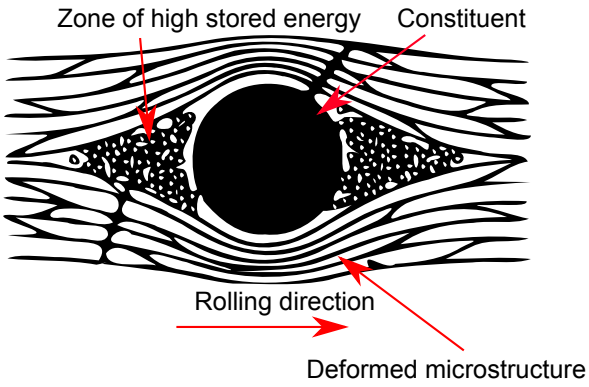

Figure 2.4.: Deformation zone around a constituent particle, showing the principle for Particle Stimulated Nucleation. Based on figure from [13].

2.3.1. Constituent particles and particle stimulated nucleation

The constituent particles are large primary particles precipitated mainly on grain boundaries during casting and solidification. The relatively large size of these particles limits their contribution to the Zener-drag (further explained in the next section), but they can still have a large impact on the recrystallization kinetics, as the particles can act as nucleation sites during recrystallization through a mechanism known as *particle stimulated nucleation*, or *PSN*[3, 12].

The underlying principle for PSN is shown in Figure 2.4. Around a constituent particle a deformation zone will develop during rolling of the material, resulting in a high energy zone surrounding the particle. This high energy zone will act as a potent nucleation site during recrystallization, and is often the dominating nucleation mechanism in commercial aluminium alloys[3]. The presence of constituent particles can thus have a large grain refining effect[10].

According to Vatne et.al[3] the particles have to be larger than a critical size, μ^*, in order to act as a nucleation site. This critical size can be expressed by the Gibbs-Thompson equation:

$$\mu^* = \frac{4\gamma_{GB}}{P_D(0) - P_Z(0)} \tag{2.1}$$

where γ_{GB} is the specific grain boundary energy between the nucleus and the deformed matrix[3]. P_D is the driving force for recrystallization, representing the stored energy in the material (explained in Sec. 2.4.4), while P_Z is the retarding force, represented by a Zener-drag. The dispersoids are normally significantly smaller than the critical size, and will therefore not act as nucleation sites.

2.3.2. Dispersoids and Zener-drag

The dispersoids are small particles precipitated mainly during the annealing process. The small size of these particles limits their utility as nucleation sites, but they will still have an impact on the recrystallization kinetics through the Zener-drag. The Zener-drag acts as a retarding force on boundary migration both during sub-grain growth, recrystallization and grain growth, as illustrated in Figure 2.5. The growing grain boundary moves unhindered

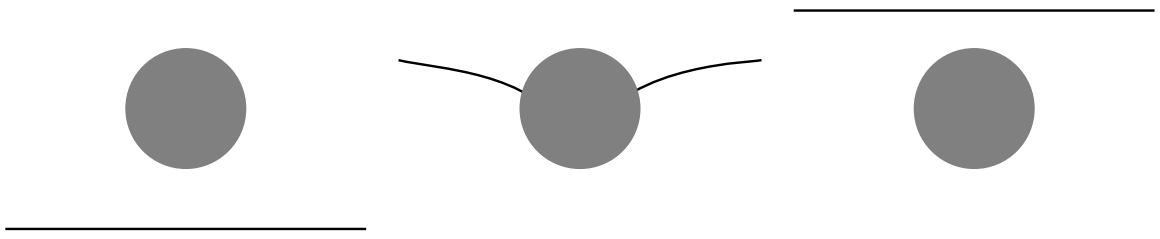

(a) $t = t_1$ (b) $t = t_2$ (c) $t = t_3$

Figure 2.5.: The effect of the Zener-drag on a growing grain boundary. The black line represents a grain boundary growing upwards. The gray circle is a small particle (dispersoid). Time is increasing from left to right, so $t_3 > t_2 > t_1$. [15]

at $t = t_1$, before $t = t_2$ where parts of the grain boundary is replaced with the particle. If migration of the boundary continues, new boundary has to be recreated, which requires energy. This is the source of the Zener-drag[10, p. 12].

The Zener-drag can be expressed by [14]:

$$P_Z = \frac{3\gamma_{GB} f_p}{2r_p} \tag{2.2}$$

where γ_{GB} is the boundary energy, f_p is the volume fraction of particles and r_p is the particle radius. This equation implies that a large volume fraction of small particles will give a large Zener-drag. Because of this the main contribution to the Zener-drag are from the small dispersoids, not from the larger constituents.

2.4. The Alsoft Model

Alsoft is a physically based model which simulates the microstructure development in an aluminium alloy during back-annealing. It is developed by NTNU/Sintef, in collaboration with Hydro Aluminium. The model is an extension of the classical Johnson-Mehl-Avrami-Kolmogorov(JMAK) approach, and which in addition to recrystallization, also simulates the effects of recovery. The model in its present form is based on works by Marthinsen, Vatne and Furu[1–3].

Only a basic overview of the model will be given here, with focus on the parts relevant to the coupling with the precipitation model. A more thorough presentation of the model, and all the equations, can be found in [3, 15–17].

2.4.1. Program structure

Alsoft is structured in the same way as Precipal (see Section 2.5.2), where a set of differential equations are solved for each time step. The program is controlled by three input files (they can also be in the same physical file separated into different categories): *alsoft.inp*

containing most of the input parameters (i,e initial values for subgrain size and dislocation density, and various constants), *alsoft.ele*, containing alloy specific parameters (i.e alloy composition, diffusivities and activation energies), and *alsoft.trt* containing information about the annealing process, and external parameters (temperature, Zener-drag and solid solution concentration at different time steps). An example of these input files can be seen in Appendix C.

After the differential equation set is solved for all the time steps specified, an output file, *alsoft.out* is produced, containing values for over 40 parameters at each time step, including fraction recrystallized, subgrain size and flow stress.

The integrator used by Alsoft is the *odeint()* function from the *scipy.integrate* library.

2.4.2. Recrystallization kinetics

The recrystallization model used in Alsoft is based on the simple mathematical model developed independently by Johnson and Mehl, Avrami, and Kolmogorov at the end of the 1930s, and is based on the following assumptions[1]:

- Random distribution of nucleation sites
- Constant grain growth rate
- Isotropic growth (i.e same growth rate in all directions)

Central in the JMAK-approach is the concept of *extended* volume fraction recrystallized, which is the volume fraction that would be recrystallized if no consideration was given to the fact that different grains would interact with each other, and eventually overlap. In the case of site-saturation nucleation kinetics (i.e all nucleation takes place at t=0), the extended volume fraction recrystallized can simply be expressed by the number of nucleation sites multiplied by the volume of the recrystallized grains:

$$X_{ext} = \overbrace{N_{tot}}^{\#\text{ Nucleation sites}} \underbrace{\frac{4}{3}\pi(Vt)^3}_{\text{Volume of recrystallized grains}} \tag{2.3}$$

where V is the growth rate of recrystallized grains and t is the time.

Due to the assumption of random distribution of nucleation sites, the change in the *real* volume fraction of recrystallized grains (i.e overlapping effect are considered) will be the same as the change in the extended volume, multiplied by the remaining untransformed volume:

$$dX = (1 - X)dX_{ext} \tag{2.4}$$

By integration and reorganization of this equation the real fraction recrystallized can be expressed as:

$$X = 1 - \exp(-X_{ext}) \tag{2.5}$$

By combination of Equation 2.3 and 2.5 real fraction recrystallized can be expressed by:

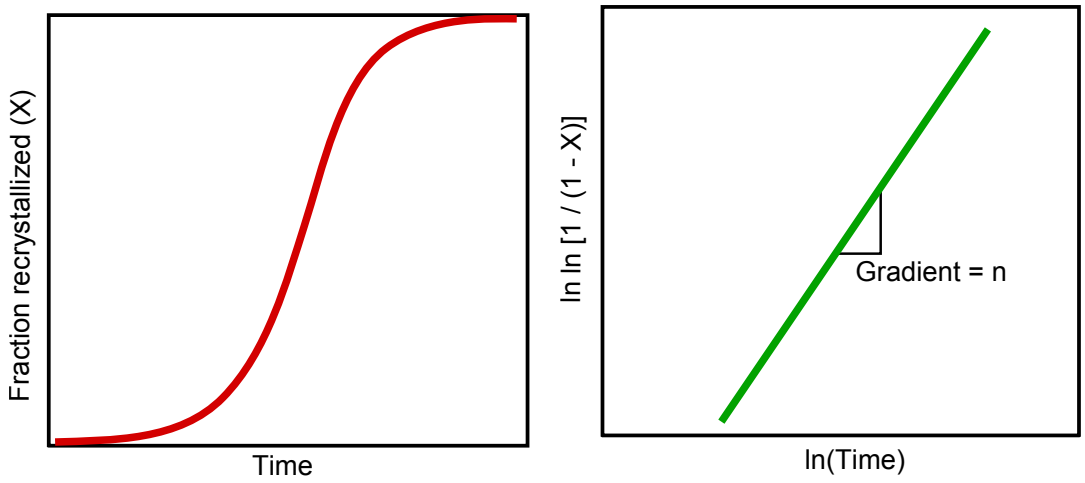

(a) Fraction recrystallized (b) Avrami plot

Figure 2.6.: Based on figure from [20].

$$X = 1 - \exp\left(-N_{tot}\frac{4}{3}\pi V^3 t^3\right) \tag{2.6}$$

By substituting $B = N_{tot}\frac{4}{3}\pi V^3$ and $n = 3$ you get the so called Johnson-Mehl-Avrami-Kolmogorov equation:

$$X = 1 - \exp(-Bt^n) \tag{2.7}$$

here n is called the Avrami constant, and is used as measure for the recrystallization kinetics. It can be interpreted as the gradient when plotting $\ln(\ln(\frac{1}{1-x}))$ vs $\ln(t)$, as illustrated in Figure 2.6. There are two special cases for the Avrami constant, n = 4 with constant nucleation and growth rate, and n = 3 at site-saturation (as assumed during the derivation of the equation) Experimental values for the Avrami constant during annealing of cold worked aluminium are often in the range 1 to 2, but exponents below 1 are also found[1, 2].

Alsoft simulations can be performed with the assumption of site-saturation nucleation, or with time-dependent nucleation, (based on theory by Zurob and Dunlop [18, 19]). In this work, however, only the site-saturation model is considered, as the time dependent model is not yet properly validated against experimental data.

2.4.3. Nucleation

For all simulations with Alsoft in this thesis site-saturation nucleation is employed. This implies that all nucleation happens simultaneously, at $t = 0$. There are three different categories of nucleation sites used in Alsoft: Particle stimulated nucleation (PSN), nucleation on old cube grains (Cube) and nucleation on grain boundaries (GB). The three nucleation site categories are summed into a single variable, N_{tot}:

$$N_{tot} = N_{PSN} + N_{cube} + N_{GB} \tag{2.8}$$

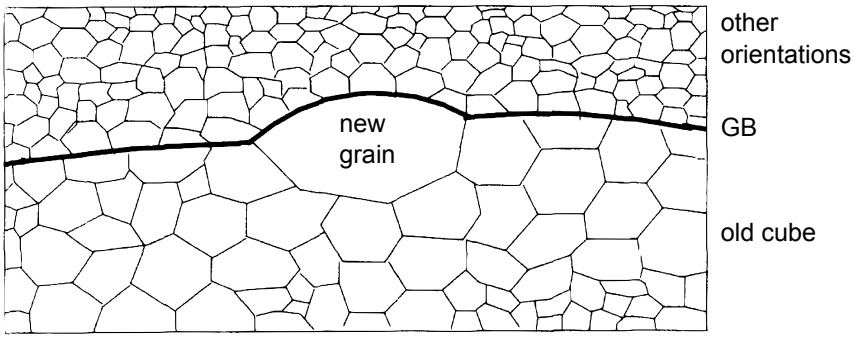

Figure 2.7.: Schematic illustration of the cube nucleation mechanism. Based on figure from [3].

The number of nucleation sites also determine the final recrystallized grain size (assuming 100 % recrystallization), which can be expressed by:

$$D(t) = \left(\frac{X(t)}{N_{tot}}\right)^{1/3} \tag{2.9}$$

Particle stimulated nucleation

PSN is often the most prominent nucleation mechanism in industrial aluminium alloys, including the AA3xxx alloy used in this thesis. The physical reasoning for PSN is explained in Section 2.3.1. The equation for the number (density) of PSN sites used in Alsoft are based on works by Vatne[3], and is expressed as:

$$N_{PSN} = C_{PSN} N_0 \exp\left(-\frac{4LC_{PE}\gamma_{GB}}{P_D(0) - P_Z(0)}\right) \tag{2.10}$$

where C_{PSN} is the number of nucleation sites per particle, and C_{PE} is a modeling constant. H_0 and L are alloy dependent constants. All these parameters are given as input to the model, and the values used can be found in Appendix C.2. $(P_D(0) - P_Z(0))$ is the net driving force for recrystallization at $t = 0$, where $P_D(0)$ is the driving force, and $P_Z(0)$ is the retarding force (as explained in Sec. 2.3.2).

The implication of this equation is that the number of PSN sites are directly dependent on the initial Zener-drag, which means that coupling of Alsoft with the precipitation model should have an effect on the grain size, especially if $P_Z(0)$ approaches $P_d(0)$ ((as can be seen in Sec. 3.5.5))

Cube

Cube grains are grains with texture of the form: {001}<001> [21, 22]. These grains will remain metastable during deformation and be elongated into cube grain bands. The subgrains inside the cube grains are generally larger than other subgrains, making these into potent nucleation sites[3]. The nucleation mechanism is illustrated in Figure 2.7, where a new grain is nucleated on the border between "old" cube grains (regions with cube texture before the deformation) and an area with another orientation. It is also

assumed that nucleation can only happen on the cube boundary when the neighbor grain has a S-deformation orientation ({123}<634>)[3].

The equation used in Alsoft to calculated the number of cube nucleation sites are based on the expression presented by Vatne[3], and is expressed as:

$$N_{cube} = C_{Cube}\delta(0)R_c(1-R_c)R_{cube}F^*_{cube}\frac{2}{D_0}\left[e^{\epsilon}+e^{-\epsilon}+1\right] \tag{2.11}$$

here C_{Cube} is a modeling constant, $\delta(0)$ is initial subgrain size and ϵ is the strain induced by the deformation process and D_0 is the mean grain size before deformation. All four parameters are given as input (see Appendix C.2). R_{cube} is the volume fraction of cube grains having S-texture grains as the closest neighbor, calculated by a sub model in Alsoft (See [3, 15, 17] for details.).

F^*_{cube} is the number of sub grains that are larger than the critical size. It is calculated by integrating over the subgrain site distribution from the normalized critical subgrain size (χ^*_{cube}) to infinity:

$$F^*_{cube} = \int_{\chi^*_{cube}}^{\inf} f_{cube}(\chi)d\chi \tag{2.12}$$

where f_{cube} is the subgrain size distribution, assumed to be a log-normal distribution with shape parameter 0.4545 (This distribution is chosen in order to match the gamma-distribution used in earlier versions of Alsoft [3], while still having an analytical solution).

The relative subgrain size is given by:

$$\chi^*_{cube} = \frac{\delta^*(0)}{\delta_{cube}(0)} \tag{2.13}$$

where δ^* is the critical subgrain size given by:

$$\delta^*(t) = \frac{4\gamma_{GB}}{P_d(0)-P_z(0)} \tag{2.14}$$

Equation 2.12 can be combined with Equation 2.13 and 2.14 and solved analytically (approximated with the error function):

$$F^*_{cube} = \frac{\operatorname{erf}\left(\log\left(\frac{4\gamma_{GB}}{\delta_{cube}(0)(P_d(0)-P_z(0))}\right)+0.5+s^2*\sqrt{2}^{-1}\right)}{2} \tag{2.15}$$

where s is the shape parameter (=0.4545). The implication of this equation is that the initial Zener-drag ($P_Z(0)$) will have an limited effect on the number of nucleation sites when the difference between $P_d(0)$ and $P_Z(0)$ is large, but if $P_Z(0)$ approaches $P_d(0)$, the number of nucleation sites will decrease dramatically, and the grain size will increase (as can be seen in Sec. 3.5.5).

Grain boundary

PSN and nucleation on old cube grains are not alone able to describe the grain sizes observed experimentally[3], it is therefore assumed that nucleation can also occur on

old grain boundaries with orientations other than the cube orientation, with a similar mechanism to the old cube grain boundaries explained above [3].

The equation used in Alsoft to calculate the number of nucleation sites is similar to the equation used for the cube sites, and is like the other nucleation equations based on works by Vatne[3]. It is expressed as:

$$N_{GB} = C_{GB}\delta(0)(1 - R_{GB})F^*_{GB}\frac{2}{D_0}\left[e^{\epsilon} + e^{-\epsilon} + 1\right] \tag{2.16}$$

where F_{GB} is the number of subgrains larger than the critical size (calculated the same way as for the cube sites, Eq. 2.12) and C_{GB} is a modeling constant given as input.

2.4.4. Evolution equations

The state-parameters in Alsoft are the subgrain size, *delta* and the dislocation density ρ (both describing recovery), and the size of recrystallized grains, d (describing recrystallization). The state parameters are expressed as a set of coupled differential equations.

Recovery

The evolution of the subgrain size and the dislocation density is described by[12, 23]:

$$\dot{\delta}(t) = -\nu_D b A_\delta B_\delta \exp\left(-\frac{U_a}{RT(t)}\right) 2\sinh\left[\frac{A_\delta}{kT(t)}Gb^4\sqrt{\delta(t)}\right], A_\delta = w_\delta C_{ss}^{-e} \tag{2.17}$$

$$\dot{\rho}(t) = -\nu_D b A_\rho B_\rho \rho(t)^{3/2} \exp\left(-\frac{U_a}{RT(t)}\right) 2\sinh\left[\frac{A_\rho}{kT(t)}(Gb^4\sqrt{\rho(t)}\right], A_\rho = w_\rho C_{ss}^{-e} \tag{2.18}$$

here v_D the Debye frequency, k is Boltzmanns constant, $B_{\delta,\rho}$ is an alloy dependent constant,$w_{\delta,\rho}$ is another constant, U_a is the activation energy for diffusion. The numerical value for these parameters can be seen in Appendix C.2. C_{ss} is the effective solid solution concentration (the sum of all elements in solid solution weighted by their respective activation energies for diffusion in aluminium), given as an external parameter. G is the shear modulus, given by a sub model in Alsoft(not described here, see [15, 17]).

These equations are based on the assumption that the rate for annihilation of dislocations are limited by atoms in solid solution retarding dislocation movement, and activation of these away from the dislocations as the rate-controlling reaction.

Recrystallization

Equation 2.17 and 2.18 are coupled through the equation for the growth rate of recrystallized grains[12]:

$$V(t) = M(T)\left[P_D(t) - P_Z(t)\right] \tag{2.19}$$

where $M(T)$ is the mobility for grain growth (given by Eq. 2.21), P_Z is the retarding force, given as an external parameter (assumed to be a Zener-drag, as described in Sec. 2.3.2) and P_D is the driving force for grain growth, calculated from its derivative:

$$\dot{P}_d = \frac{\alpha \gamma_{SB} \dot{\delta}}{\delta^2} + \frac{Gb^2 \dot{\rho}}{2} \tag{2.20}$$

here γ_{SB} is the sub grain boundary energy (based on the Read-Shockley equation, see [15, 17]) and α is a constant given as an input parameter. There are two contributions to the driving force for recrystallization, the stored energy from the subgrains (first term), and the contribution from the dislocations inside the subgrains (second term).

If the driving force for recrystallization (P_D) becomes lower than the Zener-drag (P_Z) (i.e negative net driving force for grain growth) the growth rate is set to zero, effectively stopping recrystallization. Examples of this occurring can be seen in Section 3.5.2.

The mobility for grain growth is given by:

$$M(T) = \frac{M_0}{C_{ss} kT} \exp\left(\frac{U_{rex}}{RT}\right) \tag{2.21}$$

where U_{rex} is the activation energy for recrystallization, given as a input parameter and M_0 is a constant which can be used to shift onset of recrystallization to shorter or longer times.

2.5. The Precipal Model

Precipal is a precipitation model simulating precipitation of particles during back-annealing of Al-Mn(-Fe-Si) aluminium alloys, with special attention to precipitation of Mn-containing dispersoids.

In this section all equations used in the Python implementation of Precipal are presented. The model is based on the work of Lok in his PhD thesis[6], and the existing Fortran 77 implementation of Precipal, implemented by Friis[4].

2.5.1. Model Assumptions

The precipitation model is specifically developed for Al-Mn-(Fe-Si) alloys (AA3xxx) and is based on the following assumptions[6], (following from the detailed experimental characterization carried out by Lok in his PhD thesis):

- The depletion of Mn from solid solution is by nucleation and growth of α-$Al_{12}Mn_3Si$ dispersoids and by growth of Al_6(Fe,Mn) constituents. The nucleation of constituents, and the transition between constituents and dispersoids is not modeled (i.e. the number of constituent particles are constant).

- For undeformed material, only dispersoids which form homogeneously on the grain interior, and for the deformed material, only dispersoids which nucleate heterogeneously on the subgrain boundaries, are modeled.

- Particle size distribution effects are not modeled. This means that only the average size of the particles, which are assumed to be spherical, are monitored.

- The effect of recrystallization on the precipitation kinetics is modeled by changing from rapid solute diffusion on the subgrain boundaries in the deformed material, to slower solute vacancy diffusion in the undeformed recrystallized material. The recrystallization kinetics is not modeled in Precipal, but is provided as an external parameter. The model can also be coupled with Alsoft, and in this case the fraction recrystallized will be calculated by Alsoft.

2.5.2. Program structure

Precipal is structured in the same way as Alsoft, in which a set of differential equations are solved numerically at each time step. The program is controlled by three input files(can also be specified by one physical file divided into different categories); *precipal.inp* where most input parameters are specified, *precipal.ele* where most alloy specific parameters are defined (i.e alloy composition, activation energies and diffusivity prefactors), and *precipal.trt* in which information about the annealing process are specified (time and temperature) in addition to external parameters (fraction recrystallized and sub grain size). An example of these input files can be found in Appendix C.

When Precipal is executed the differential equations are solved numerically for each time step by the *odeint()* function from the *scipy.integrate* library. After the equations have been solved an output file will be generated, containing data for over 30 different parameters at each time-step, including the radius, volume fraction and number density of dispersoids and constituents.

2.5.3. Evolution Equations

In the Fortran 77 implementation of Precipal the system was described by three state parameters, N_d, f_d and f_c, representing the number and volume fraction of dispersoids, and the volume fraction of constituents. In Precipal the system can be described by the same equations, or by an equivalent set of equations which use particle radii instead of volume fractions as state parameters. The derivation of these equations, and the consistency between them, is shown in Appendix A.1 and Section 3.1.

The state parameters are described by a set of differential equation, either by Equations 2.22 - 2.24, or by Equations 2.22, 2.25 and 2.26:

Number of dispersoids:

$$\frac{dN_d}{dt} = X j_d(D^L_{\mathrm{Mn}}) + (1-X) j_d(D^{eff}_{\mathrm{Mn}}) \tag{2.22}$$

Volume fraction:

$$\begin{aligned}\frac{df_d}{dt} = {} & X\left(4\pi r_d^2 s_d N_d v_d(D^L_{\mathrm{Mn}}) + \frac{4\pi r^3}{3} j_d(D^L_{\mathrm{Mn}})\right) \\ & + (1-X)\left(4\pi r_d^2 s_d N_d v_d(D^{eff}_{\mathrm{Mn}}) + \frac{4\pi r^3}{3} j_d(D^{eff}_{\mathrm{Mn}})\right)\end{aligned} \tag{2.23}$$

$$\frac{df_c}{dt} = X 4\pi r_c^2 s_c N_c v_c(D^L_{\mathrm{Mn}}) + (1-X) 4\pi r_c^2 s_c N_c v_c(D^{eff}_{\mathrm{Mn}}) \tag{2.24}$$

Radius:

$$\frac{dr_d}{dt} = Xv_d(D^L_{\mathrm{Mn}}) + (1-X)v_d(D^{eff}_{\mathrm{Mn}}) \tag{2.25}$$

$$\frac{dr_c}{dt} = Xv_c(D^L_{\mathrm{Mn}}) + (1-X)v_c(D^{eff}_{\mathrm{Mn}}) \tag{2.26}$$

In Equation 2.22 - 2.26 X is volume fraction recrystallized, given as an external input parameter. All these equations are expressed as a weighted average between the volume fraction undeformed material (multiplied by X), and the volume fraction of deformed material (multiplied by $(1-X)$). D^L_{Mn} and D^{eff}_{Mn} are the diffusivity in the lattice and effective diffusivity, respectively. They are given by equation 2.28 and 2.30 below. j_d is the nucleation rate of dispersoids, given by Equation 2.32 below. r_d and r_c is the radius of dispersoids and constituents, respectively. s_d and s_c are factors accounting for the size distribution of the dispersoid and constituent particles, both are set to one for all simulations presented in this thesis. v_d and v_c are the growth rates of dispersoids and constituents, given by Equation 2.40 and 2.41 below. N_c is the number of constituent particles, and is treated as a constant(for a given alloy), and due to this there is no nucleation equation for the constituent particles.

r_d and r_c in Equation 2.23 and 2.24 are calculated by the simple geometric relationship between the radius, volume fraction, and number of dispersoids (by assuming spherical particles):

$$r = \left(\frac{3f}{4\pi sN}\right)^{1/3} \tag{2.27}$$

Diffusivities

As stated in Section 2.5.1 there are two different mechanisms for nucleation and growth of particles simulated in Precipal, namely, nucleation and growth homogeneously in the lattice, or nucleation and growth on subgrain boundaries. Since both the nucleation and growth of particles are assumed to be diffusion controlled, the defining distinction between the two mechanisms (in regards to Precipal simulation) are the diffusivities, with significantly faster diffusion on the subgrain boundaries.

The two diffusivities are given as a standard Arrhenius temperature dependence:

$$D^L_{\mathrm{Mn}} = D^{0,L}_{\mathrm{Mn}} \exp\left(-\frac{Q^{D,L}_{\mathrm{Mn}}}{RT}\right) \tag{2.28}$$

$$D^{SGB}_{\mathrm{Mn}} = D^{0,SGB}_{\mathrm{Mn}} \exp\left(-\frac{Q^{D,SGB}_{\mathrm{Mn}}}{RT}\right) \tag{2.29}$$

with both the prefactors ($D^{0,L}_{\mathrm{Mn}}$, $D^{0,SGB}_{\mathrm{Mn}}$), and activation energies ($Q^{D,L}_{\mathrm{Mn}}$, $Q^{D,SGB}_{\mathrm{Mn}}$), given as input parameters.

Due to the assumption that all nucleation and growth of particles take place in the matrix for undeformed material, and on the subgrain boundaries in the deformed material, the effective diffusivity can simply be expressed as a weighted average (weighted by the volume fraction of subgrains) between the diffusivity in the lattice and on the subgrain boundary:

$$D_{\mathrm{Mn}}^{eff} = (1 - f_{SGB})D_{\mathrm{Mn}}^{L} + f_{SGB}D_{\mathrm{Mn}}^{SGB} \tag{2.30}$$

where the fraction of subgrain boundary, f_{SGB}, is given by the width of the subgrain boundaries t_{SGB} (given as input) divided by the average subgrain size (given as an external parameter):

$$f_{SGB} = \frac{t_{SGB}}{\delta} \tag{2.31}$$

2.5.4. Nucleation and Growth Rates

Nucleation rates

The nucleation rate of dispersoids, as a function of diffusivity, is given by [6]:

$$j_d(D) = N_{het}^{tot}\beta^*(D)Z \exp\left(-\frac{\Delta G_{het}^*}{kT}\right) \exp\left(-\frac{\tau(D)}{t}\right) \tag{2.32}$$

here N_{het}^{tot} is the number density of available nucleation sites for heterogeneous nucleation, given by Equation 2.33 below. $B^*(D)$ represents the rate at which atoms are attached to a critically sized dispersoid nucleus, as a function of diffusivity[6], given by Equation 2.34 below. The Zeldovic factor, Z, corrects for nuclei that grow beyond the critical size[6], and is given as input. ΔG_{het}^* is the activation energy associated with heterogeneous nucleation, given by Equation 2.38 below. k is Boltzmann constant, T is the annealing temperature and t is the time. $\tau(D)$ is a characteristic incubation time before steady state nucleation rate is obtained, given by Equation 2.39 bellow.

The number of constituent particles are assumed to be constant (i.e the nucleation rate for constituent particles, j_c, is zero.)

The number density of heterogeneous nucleation sites in the deformed state are given by:

$$N_{het}^{tot} = f_{SGB}N_{hom}^{tot} \tag{2.33}$$

where N_{hom}^{tot} is the number density of homogeneous nucleation sites. The effect of this equation is that the number of heterogeneous nucleation sites is significantly lower than the number of homogeneous sites.

The rate at which atoms are attached to a critically sized nucleus is given by [6]:

$$\beta^*(D) = \frac{6\pi D r_d^{*2} C_{\mathrm{Mn}}}{a_0^4} \tag{2.34}$$

where C_{Mn} is the Mn concentration in solid solution (from Eq 2.51), a_0 is the lattice parameter for aluminium (input parameter) and r_d^* is the critical dispersoid radius (i.e the minimum size a dispersoid nuclei can have in order to continue to grow) given by:

$$r_d^* = \frac{2\gamma_d}{\Delta G_v} \tag{2.35}$$

where γ_d is the specific surface energy between the dispersoid and the matrix (input parameter) and ΔG_v is the net decrease in Gibbs free energy when a stable precipitate

nucleus is formed (i.e the difference in free energy between the newly created nucleus and the same volume of super saturated matrix), and can be expressed by[6]:

$$\Delta G_v = \frac{RT}{V_m^d} \ln\left(\frac{C_{\text{Mn}}}{C_{\text{Mn}}^{eq}}\right) \tag{2.36}$$

here C_{Mn}^{eq} is the equilibrium solubility of Mn (given by Eq. 2.44 below), and V_m^d is the molar volume of an dispersoid (i.e the volume of one mol of $Al_{12}Mn_3Si$), given as an input parameter.

The activation energy for homogenous nucleation is the energy barrier a critically sized dispersoid nuclei has to overcome in order to continue to grow, and is given by [6]:

$$\Delta G_{hom}^* = \frac{16\pi\gamma_d^3}{3\Delta G_v^2} \tag{2.37}$$

Heterogeneous nucleation is inherently a complex process. Due to this the activation energy for heterogeneous nucleation is hard to describe properly. In Precipal this is simplified into a factor, η, which specifies the ratio between the activation energies for heterogeneous and homogeneous nucleation (given as an input parameter between 0 and 1) [6]. The activation energy for heterogeneous nucleation can thus be expressed by:

$$\Delta G_{het}^* = \xi \Delta G_{hom}^* \tag{2.38}$$

The characteristic incubation time before steady state nucleation of dispersoids is expressed by:

$$\tau(D) = \frac{1}{2\beta^*(D)Z} \tag{2.39}$$

Growth rates

The growth rates of dispersoids and constituents are given by:

$$v_d(D) = \frac{D}{r_d} \frac{C_{\text{Mn},d}^{\lambda} - C_{\text{Mn},d}^{i}}{C_{\text{Mn},d}^{p} - C_{\text{Mn},d}^{i}} \tag{2.40}$$

$$v_c(D) = \frac{D}{r_c} \frac{C_{\text{Mn},c}^{\lambda} - C_{\text{Mn},c}^{i}}{C_{\text{Mn},c}^{p} - C_{\text{Mn},c}^{i}} \tag{2.41}$$

The physical interpretation of the different concentrations in the growth rate equations can be seen in Figure 2.8a. $C_{\text{Mn},d,c}^{i}$ is the equilibrium solute concentration at the particle-matrix interface, given by Equation 2.42 and 2.43 (below) for dispersoids and constituents, respectively. $C_{\text{Mn},d,c}^{p}$ is the Mn concentration inside the particles, and is assumed to be the stoichiometric concentrations. $C_{\text{Mn},d}^{\lambda}$ and $C_{\text{Mn},c}^{\lambda}$ is the concentration on the surrounding volume boundary illustrated in Figure 2.8b, and is given by Equation 2.45 and 2.46 (below) for dispersoids and constituents, respectively.

The equilibrium solute concentration at the dispersoid-matrix interface (illustrated in Fig. 2.8a) is given by the overall equilibrium solubility, C_{Mn}^{eq}, corrected for the curvature of the dispersoids[6]:

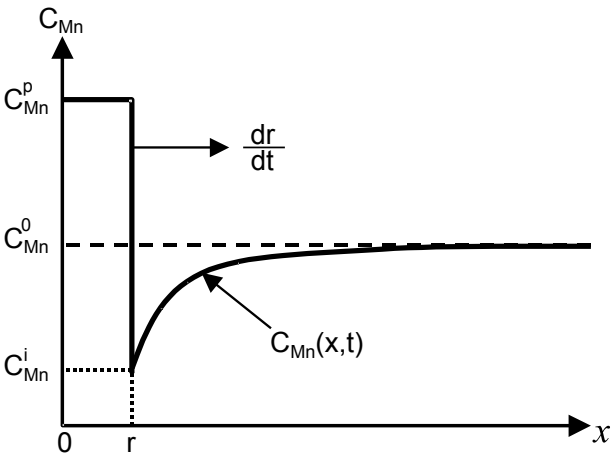

(a) Mn concentration profile inside and outside particle. C^p_{Mn} is the constant solute concentration inside the particle, C^0_{Mn} is the initial solid solution concentration and C^i_{Mn} is the equilibrium solute concentration at the particle-matrix interface. $C_{Mn}(x,t)$ is the solute concentration profile outside the particle.

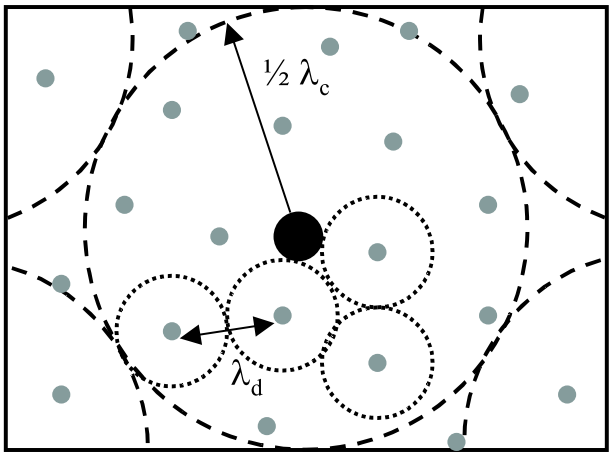

(b) Schematic illustration of the dispersoid and constituent distribution. λ_d and λ_c is the average distance between dispersoids and constituent, respectively.

Figure 2.8.: Based on figure from [6, p. 86]

$$C^i_{\mathrm{Mn},d} = C^{eq}_{\mathrm{Mn}} \exp\left(\frac{2\gamma_d V^d_m}{r_d RT}\right) \tag{2.42}$$

where γ_d is the specific surface energy between the dispersoid and the matrix, R is the universal gas constant and V^d_m is, as mentioned earlier, the molar volume of a dispersoid (i.e the volume of one mol of $Al_{12}Mn_3Si$).

Due to the significantly larger size of the constituent particles (compared with the dispersoids), the curvature effects can be neglected so that the equilibrium solute concentration at the constituent-matrix interface can be approximated to the overall Mn equilibrium solubility:

$$C^i_{\mathrm{Mn},c} \approx C^{eq}_{\mathrm{Mn}} \tag{2.43}$$

The overall Mn equilibrium solubility is expressed as a standard Arrhenius temperature dependence:

$$C^{eq}_{\mathrm{Mn}} = C^s_{\mathrm{Mn}} \exp\left(-\frac{Q^C_{\mathrm{Mn}}}{RT}\right) \tag{2.44}$$

where C^s_{Mn} is the prefactor for equilibrium solubility and Q^C_{Mn} is the activation energy for solubility. Both parameters are given as input parameters in the element file.

The Mn concentration on the surrounding volume boundary, illustrated in Figure 2.8b, are given by[6]:

$$C^{\lambda}_{\mathrm{Mn},d} = \frac{8r_d^3 C^{p}_{\mathrm{Mn},d} - \lambda_d^3 C^{0}_{\mathrm{Mn},d} + 3r_d(\lambda_d^2 - 4r_d^2)C^{i}_{\mathrm{Mn},d}}{\lambda_d^2(3r_d - \lambda_d) - 4r_d^3} \tag{2.45}$$

$$C^{\lambda}_{\mathrm{Mn},c} = \frac{8r_c^3 C^{p}_{\mathrm{Mn},c} - \lambda_c^3 C^{0}_{\mathrm{Mn},c} + 3r_c(\lambda_c^2 - 4r_c^2)C^{i}_{\mathrm{Mn},c}}{\lambda_c^2(3r_c - \lambda_c) - 4r_c^3} \tag{2.46}$$

for dispersoids and constituent, respectively. Here λ_d and λ_c are the average distance between dispersoids and constituent (as illustrated in Figure 2.8b), and are approximated by:

$$\lambda_d = \left(\frac{6}{\pi N_d}\right)^{1/3} \tag{2.47}$$

$$\lambda_c = \left(\frac{6}{\pi N_c}\right)^{1/3} \tag{2.48}$$

In Equation 2.45 and 2.45 $C^{0}_{\mathrm{Mn},d}$ and $C^{0}_{\mathrm{Mn},c}$ is the Mn solute concentration when all the dispersoids or constituents, respectively, are dissolved (Illustrated in Figure 2.8a), and can be expressed by [6]:

$$C^{0}_{\mathrm{Mn},d} = \frac{8r_d^3 C^{p}_{\mathrm{Mn},d} + (\lambda_d^3 - 8r_d^3)C_{\mathrm{Mn}}}{\lambda_d^3} \tag{2.49}$$

$$C^{0}_{\mathrm{Mn},c} = \frac{8r_c^3 C^{p}_{\mathrm{Mn},c} + (\lambda_c^3 - 8r_c^3)C_{\mathrm{Mn}}}{\lambda_c^3} \tag{2.50}$$

where C_{Mn} is the overall solid solution content of Mn, given by the mass balance:

$$C_{\mathrm{Mn}} = \frac{(C^{0}_{\mathrm{Mn}} + C^{0}_{\mathrm{Fe}})\lambda_c^3 - 8C^{p}_{\mathrm{Mn},c}r_c^3 - 8\frac{N_d}{N_c}C^{p}_{\mathrm{Mn},d}r_d^3}{\lambda_c^3 - 8r_c^3 - 8\frac{N_d}{N_c}r_d^3} \tag{2.51}$$

where C^{0}_{Mn} and C^{0}_{Fe} are the nominal alloy concentrations of Mn and Fe (not to be confused with $C^{0}_{\mathrm{Mn},d}$ and $C^{0}_{\mathrm{Mn},c}$, which are the solute concentration when all dispersoids and constituents, respectively, are dissolved), given as input in the element file.

2.5.5. Phenomenological model

Experimental evidence suggests that precipitation of dispersoid during back annealing can not be properly described by the precipitation model described above. This can be seen from the experimental data presented in the doctoral thesis of Lok[6]. The source of this discrepancy is currently unknown, but several possible explanations are presented by Lok[6].

Due to the unknown source of the discrepancy between the simulated results and the experimental data a ”phenomenological model” was introduced into Precipal, based on the model presented by Lok. In this model nucleation of dispersoids is simplified as site-saturation nucleation, with no incubation time (i.e all nucleation at $t = 0$). The number of dispersoids is thus constant, and is provided as an input parameter based on experimental data[6].

In the phenomenological model two empirical fitting parameters are introduced into the growth equations for dispersoids and constituent, n, and θ, leading to the following expression for the growth rates:

$$\frac{dr}{dt} = \theta^{n-1}\left(\frac{1}{r^n} - \frac{1}{r_{\max}^n}\right)\left(\frac{D}{c_{\mathrm{Mn}}^p - c_i^{eq}}\right) \tag{2.52}$$

where $r_{\max}$ is given by:

$$r_{\max} = \frac{\lambda}{2}\left(\frac{c_0^i - c_i^{eq}}{c_{\mathrm{Mn}}^p - c_i^{eq}}\right)^{\frac{1}{3}} \tag{2.53}$$

The fitting parameters for the undeformed material θ_d^u, and θ_c^u, are expressed as a function of the number of dispersoids, N_d, and the temperature, T, respectively. The reason for the dependence on number of dispersoids can be seen by integration of Equation 2.52 without the $r_{\max}^{-m}$ term by assuming that $C_{\mathrm{Mn}} >> c_i^{eq}$, and thus also $r << r_{\max}$ (this assumption is valid for low t), and combining with the expression for volume fraction of dispersoids (Eq. A.2) [6]:

$$f = \frac{4\pi}{3}r^3 N = \frac{4\pi}{3}\left(\frac{(n+1)\theta^{n-1}Dt}{c_{\mathrm{Mn}}^p - c_i^{eq}}\right)N \tag{2.54}$$

solving for θ gives the following proportionalities for constant T and N, respectively [6]:

$$\theta(N) \propto N^{-\frac{1}{3}}\left(\frac{n+1}{n-1}\right) \tag{2.55}$$

$$\theta(T) \propto \left(\frac{D(T)}{c_{\mathrm{Mn}}^p - c_i^{eq}(T)}\right)^{\frac{-1}{n-1}} \tag{2.56}$$

The number of constituents is constant for all simulations in such a way that θ_c^u can be independent of N_c, and SEM measurements indicate that the temperature has a small impact on precipitation of dispersoids[6]. This leads to the N_d dependence for θ_d^u and T dependence for θ_d^u as shown in Table 3.4 (see Section 3.4.2, with the exponential term originating from the Arrhenius equations for D and c_i^{eq}).

The determination of the fitting parameters are explained in Section 3.4.2.

2.6. Coupling of Alsoft and Precipal

Precipal and Alsoft are coupled through their external parameters. The external parameters in Precipal, fraction recrystallized and subgrains size, are now calculated by Alsoft, and the external parameters in Alsoft, Zener-drag and effective solid solution concentration, are now calculated by Precipal (it should be noted that no Zener-drag is actually calculated in Precipal, but rather information about particle distribution and sizes are transferred to Alsoft where this information is used to calculate the Zener-drag).

The coupling is carried out by a third program, *Alprec*, which creates Alsoft and Precipal object instances, and solves the two sets of differential equations simultaneously. In these objects the reference to the function for getting the external parameters are changed to

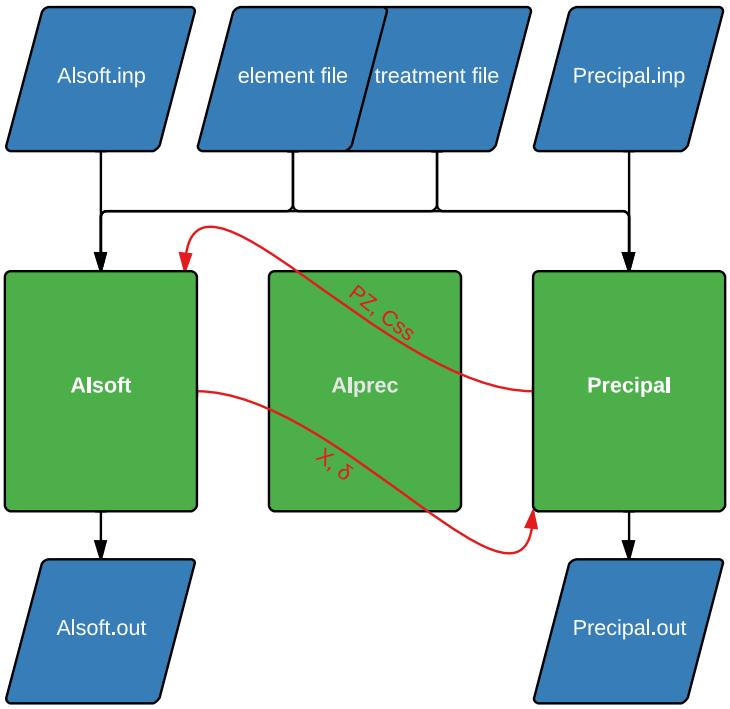

Figure 2.9.: Overview of the coupling between Alsoft and Precipal. The red arrows indicate the parameters shared by the coupling. Zener-drag (P_Z) and solid solution concentration (C_{ss}) from Precipal to Alsoft, and fraction recrystallized (X) and subgrain size (δ) from Alsoft to Precipal.

functions in Alprec which retrieves the calculated values for the external parameters from either Alsoft or Precipal. An overview of the program structure is shown in Figure 2.9. Standard input parameters for Precipal and Alsoft are used, as shown in Appendix C.

The input is handled with separate input files for Alsoft and Precipal (the same input file as when the programs are run separately), and shared element and treatment files. The treatment file now only contains the time and temperature for the annealing process, as the other external parameters are calculated by the coupling. The element file is identical to the one used by Alsoft and Precipal. Two separate output files are produced, containing the same parameters as when the models are executed separately.

The advantage of doing the coupling in this way is that only minor changes to Alsoft are necessary, i.e it can still be executed and further developed independently. The changes done to the Alsoft code are documented in Appendix B. Precipal was developed with regard to the coupling, so no changes to the program was necessary.

3. Simulations

In this chapter results from simulations will be presented. In the first two sections the new Python implementation of Precipal is compared with the original Fortran implementation, while in Section 3.3 the effect of different input parameters on Precipal are presented(i.e a parameter sensitivity test). In Section 3.4 Precipal simulations are compared with simulations performed by Lok[6]. Section 3.5 presents simulation results form the coupling of Precipal and Alsoft, and compares these results with experimental data.

All Precipal simulations are, if not otherwise stated, carried out with the Python implementation, and a standard set of reference input parameters presented in Appendix C.1. This input represents an undeformed Al-1.11wt%Mn-0.51wt%Fe-0.06wt%Si alloy annealed at a temperature of 405°C. This input is chosen to be as similar as possible to the input parameters used in the doctoral thesis of Lok [6, chap 5.3], but with some discrepancies due to differences in the model (further explained in Section 3.4).

The input used in the Alsoft simulations are described in Section 3.5, and the standard input used can be seen in Appendix C.2.

3.1. Different evolution equations

Precipal was modified to use two sets of equivalent evolution equations, either the number density of dispersoids and the *volume fraction* of dispersoids and constituents (Eq. 2.22, 2.23 and 2.24), or the number density of dispersoids and the *radius* of dispersoids and constituents (Eq. 2.22, 2.25 and 2.26).

The original expressions (used in the Fortran implementation) was chosen as they where easier to solve numerically than the new equations. With the differential equation solver used in the Python implementation this is no longer a necessity, so the new, easier, expressions can now be used. However, the original expressions was found to be more numerically stable with some combinations of input parameters, so the ability to use the old expressions is kept as an option.

The two sets of differential equations require different initial conditions. The initial conditions can be converted by using:

$$r_0 = \left(\frac{3 f_0}{4 \pi N_0} \right)^{1/3} \tag{3.1}$$

where r_0 is the initial particle radius, f_0 is the initial particle volume fraction, and N_0 is the initial number density of particles.

Table 3.1 shows equivalent initial values for both set of equations, and Figure 3.1 compares results calculated with the two equation sets. As expected and argued the results are identical. This implies that any of the two variants can be interchangeably used.

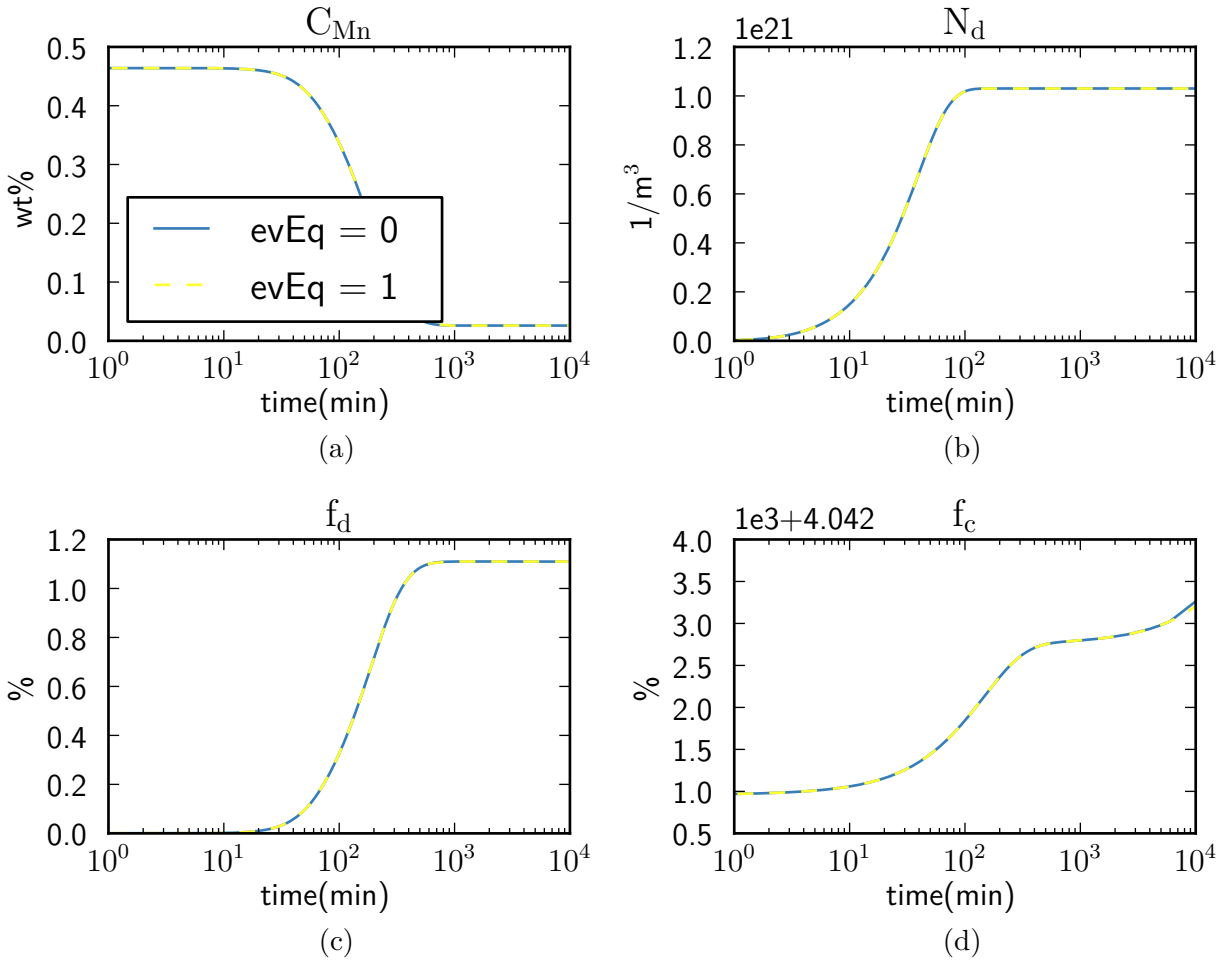

Figure 3.1.: Comparison between the two sets of differential equations, volume fraction of particles (evEq = 0), and radius of particles (evEq = 1); with initial conditions from Table 3.1.

Table 3.1.: Equivalent input parameters for the two sets of differential equations. Calculated with Equation 3.1.

Variable	Value	Unit
N_{d0}	0	$1/m^3$
N_c	6.87×10^{15}	$1/m^3$
f_{d0}	0	1
f_{c0}	0.0404	1
r_{d0}	0	m
r_{c0}	1.12×10^{-6}	m

3.2. Validation of the Python code vs original Fortran 77 implementation of Precipal

The original implementation of the Precipal model was developed in Fortran 77. In this thesis the program was rewritten in Python 2.7. The motivation for reimplementing Precipal in Python was to make it easier to couple Precipal with the softening model Alsoft (which is a Python application). The conversion was done such that the original input files could still be used.

Some changes was done to the Precipal model during the conversion, most notably the Fortran 77 version of Precipal uses a different expression for the volume fraction of dispersoids:

$$\begin{aligned}\frac{df_d}{dt} = X\left(4\pi r_d^2 s_d N_d v_d(D_{\mathrm{Mn}}^L) + \frac{4\pi(\eta r^*)^3}{3} j_d(D_{\mathrm{Mn}}^L)\right) \\ + (1-X)\left(4\pi r_d^2 s_d N_d v_d(D_{\mathrm{Mn}}^{eff}) + \frac{4\pi \eta r^{*3}}{3} j_d(D_{\mathrm{Mn}}^{eff})\right)\end{aligned} \tag{3.2}$$

The dispersoid radius, r_d, has been replaced with a constant, η, set to 1.05, multiplied by the critical radius for nucleation, r^*, given by Equation 2.35. This expression was used to make the differential equation problem easier to solve, but it is not necessary with the modern differential equation solver used in the Python implementation.

Figure 3.2 shows Precipal simulations compared with results from Fortran 77 simulations performed by Friis[4]. The Precipal simulations are using the same input parameters as the Fortran 77 simulations, input presented in the documentation of the Fortran 77 implementation[4] (not the same as used in the rest of this thesis).

In order to test the accordance between the two implementations, the Python implementation was modified to use the same expression for the evolution of the volume fraction of dispersoids. When this expression is used the results are identical. When the new expression is used the results are mostly similar, but the simulated number density of dispersoids are somewhat lower, and the shape of the volume fraction of dispersoids and solid solution concentration curves differ some (but well within the uncertainty of the model).

The conclusion from these results is that the Python implementation produces the same results with the same input as the old Fortran 77 implementation.

3.3. Parameter sensitivity

In this section the effect of different input parameters in the Precipal Mode are explored. One parameter is varied, while all other parameters are kept constant between simulations. The motivation for this sensitivity study are the uncertainty in many of the input parameters, and by performing this test the parameters having the most effect on the simulation results can be identified.

The standard input parameters in Appendix C are used.

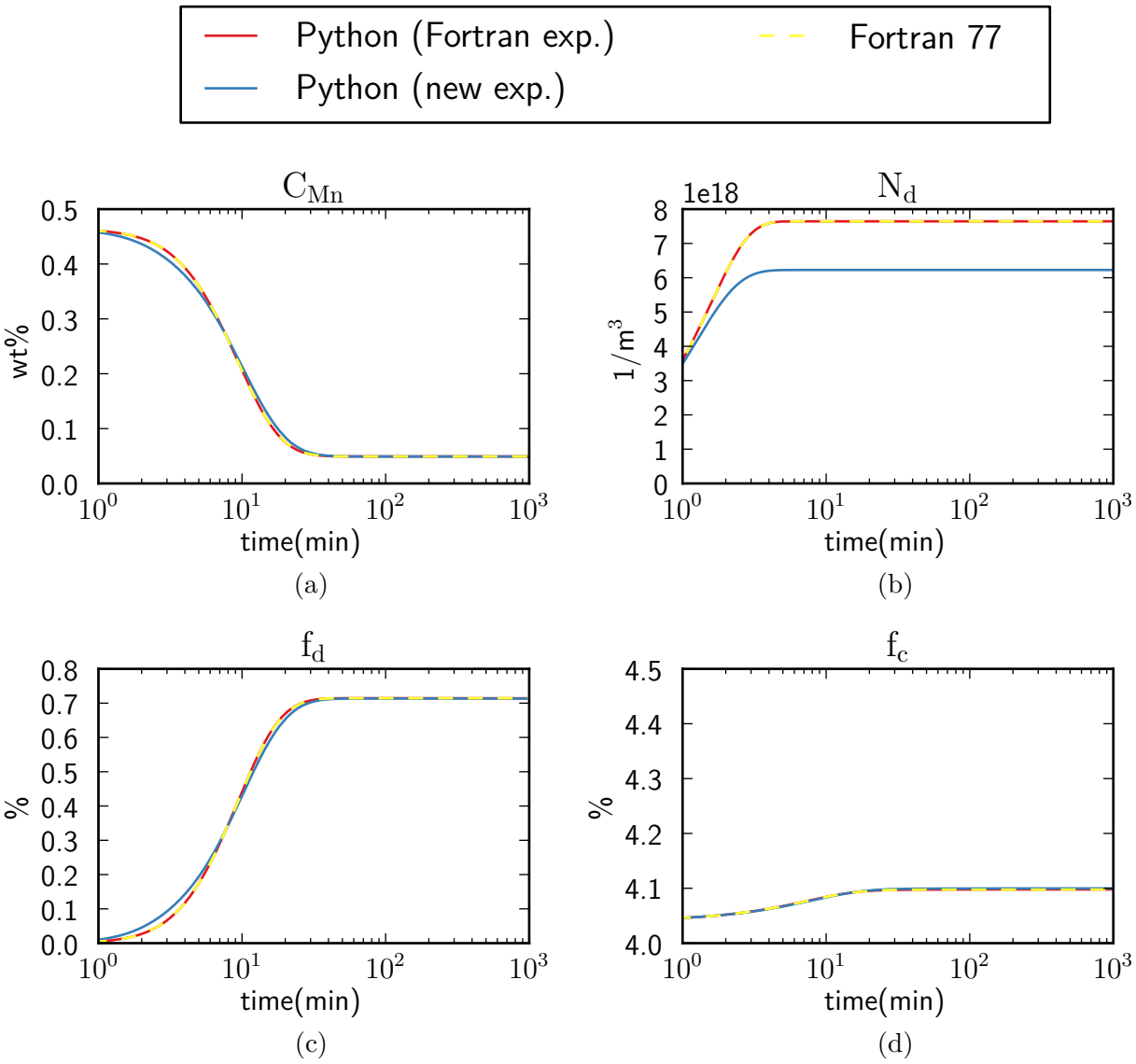

Figure 3.2.: Comparison between Fortran and Python implementations of Precipal.

3.3.1. Prefactor for equilibrium solubility (C^s)

The value for the prefactor for equilibrium solubility, C^s (Eq. 2.44) is based on the value used by Lok[6], as explained in Section 3.4. However due to the challenges of correctly converting the values used by Lok into the correct units used in Precipal (as explained in Sec. 3.4) the numerical value for C^s is not unambiguously defined, and an sensitivity test of this parameter seems therefor reasonable.

The results from simulations with varying prefactor for equilibrium solubility are shown in Figure 3.3a, 3.3c and 3.3e. A higher prefactor gives slower precipitation, and the Mn concentration in solid solution at the end increases (the equilibrium solubility). A small increase in the prefactor results in a large decrease in the final number of dispersoids. A increase in C_s from 20 to 50 atomic fraction leads to a decrease in the final number of dispersoids of three orders of magnitude. The final volume fraction of dispersoids also decreases, but only from 1.1 to 0.9 %.

3.3.2. Interface energy modifier (ξ)

The Interface energy modifier, ξ (Eq. 2.38) is a dimensionless parameter used to greatly simplify the complex interaction between a precipitate and a dislocation, and due to this its numerical value is inherently uncertain. A sensitivity study is therefor in order.

Results from simulations with varying interface energy modifier can be observed in Figure 3.3b, 3.3d and 3.3f. A decrease in the interface energy modifier leads to longer incubation time before the number of dispersoids start to grow, and the final number of dispersoids increases by about two orders of magnitude when ξ is decreased from 1 to 0.6. The initial and final concentration of Mn in solid solution is unchanged, but starts to drop later at higher values. The final volume fraction of dispersoids is almost unchanged.

3.3.3. Mn concentration in dispersoids and constituents (C_d^p, C_c^p)

The Mn concentration inside the dispersoids should in principle be given by the stoichiometric composition. As explained in Section 3.4 this does not correspond with the values used by Lok. Due to this a sensitivity study was performed.

Figure 3.4 shows results from simulations with varying Mn concentration in dispersoids (C_d^p) and constituents (C_c^p). Variation of the Mn concentration in the dispersoids has limited effect on the Mn concentration in solid solution, and the number of dispersoids, but the the volume fraction of dispersoids decreases with increasing C_d^p.

Variation of the Mn concentration in constituents (C_c^p) has a larger impact on the results than variation of the Mn concentration in the dispersoids(C_d^p). The Mn concentration in solid solution, the final number of dispersoids and the volume fraction of dispersoids decreases with increasing C_c, and the incubation time before the dispersoids starts to grow increases. The final number of dispersoids decreases with about 3 orders of magnitude, while the volume fraction of dispersoids goes from 1.6 to 0.3 %. The final Mn concentration in solid solution is unchanged.

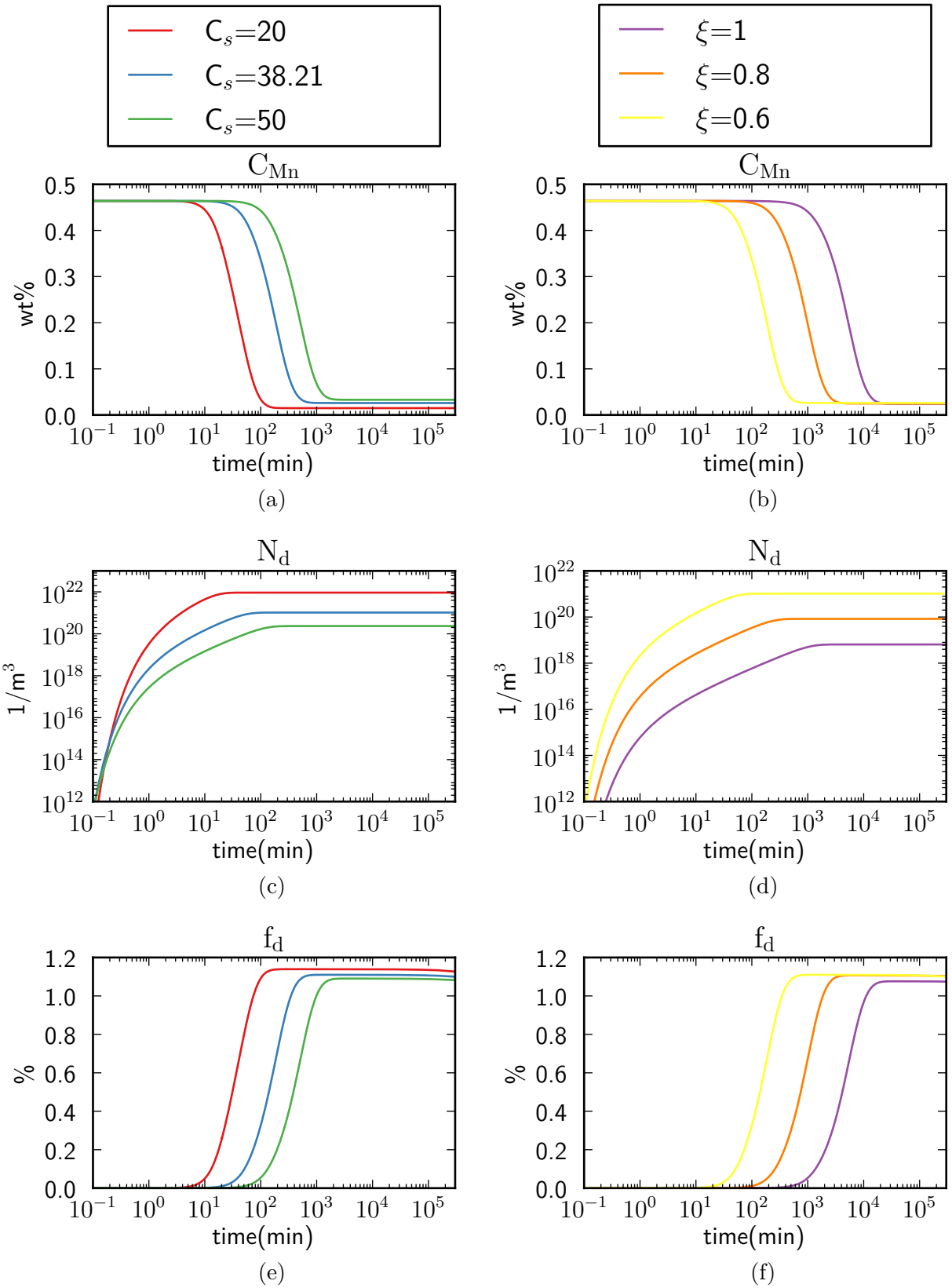

Figure 3.3.: A sensitivity study of the prefactor for equilibrium solubility of Mn, C_s, (left figures) and the interface energy modifier, ξ (right figures). Cs is stated in atomic fraction.

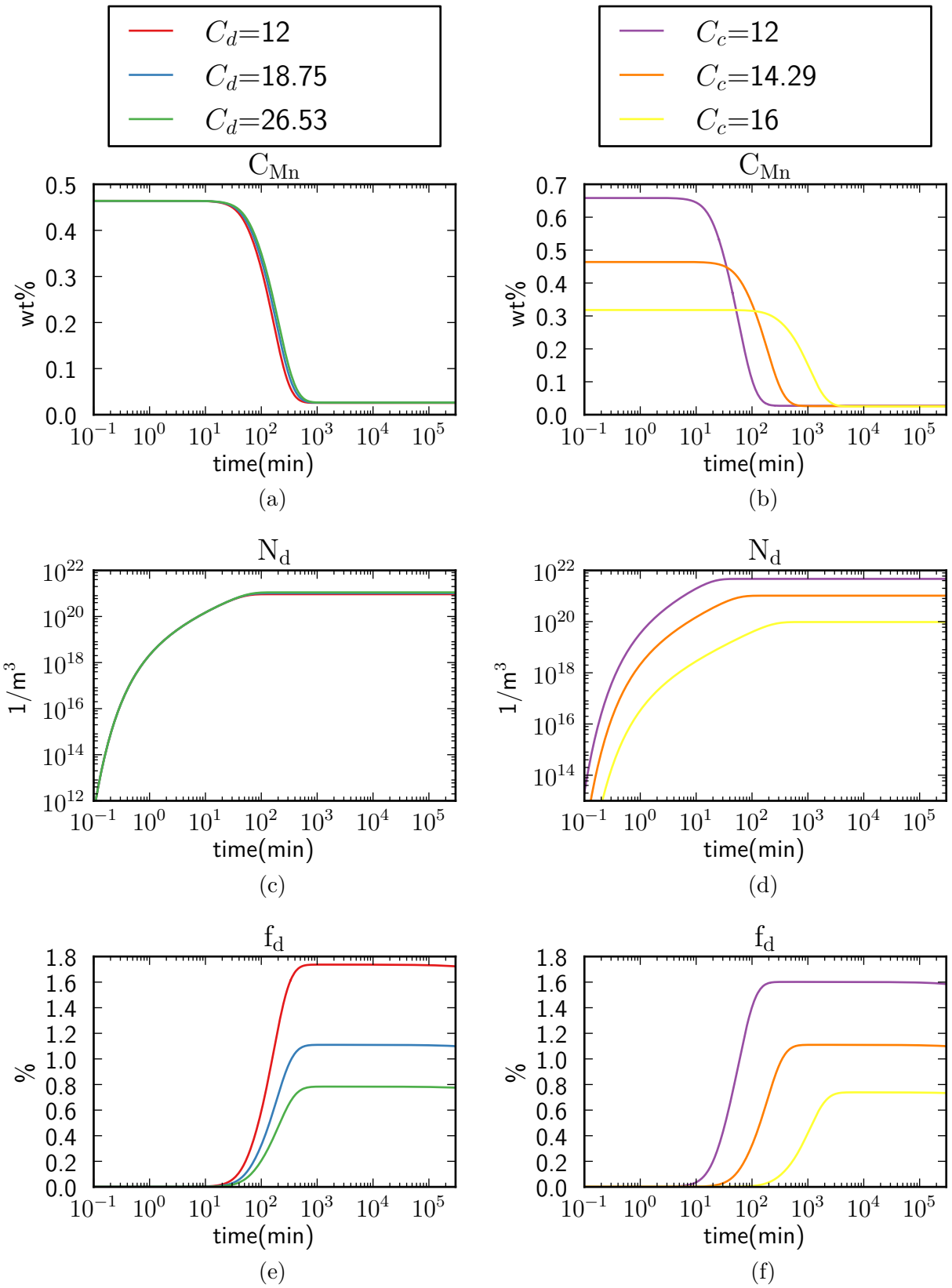

Figure 3.4.: A sensitivity study of Mn concentration in dispersoids, C_d, and in constituents, C_c. Both concentrations are stated in at%.

3.3.4. Initial number of dispersoids (N_{d0})

The value for the initial number of dispersoids, N_{d0}, is not explicitly stated in Lok[6] for all his simulations. Due to this a sensitivity study of this parameter is also appropriate.

Results from simulations with different number of initial dispersoids is shown in Figure 3.5. Varying the initial number of dispersoids has limited effect on the precipitation kinetics The only change is the initial number of dispersoids, and after precipitation starts the development in the number of dispersoids is the same for all three cases. The variations have no effect on the volume fraction of dispersoids, or the Mn concentration in solid solution.

3.3.5. Annealing temperature (T)

The temperature at which the annealing is performed is expected to have a large impact on the precipitation course, and one of the main goals of Precipal is to be able to predict the effects of different annealing temperatures. Due to this simulations with different annealing temperatures where carried out.

Undeformed material

In Figure 3.6a the Mn concentration in solid solution, number of dispersoids and volume fraction of dispersoids from Precipal simulations at different temperatures from 350 to 450 °C for undeformed (reference) material are shown. Higher annealing temperatures leads to higher equilibrium solubility (as expected based on the Arrhenius temperature dependence, Eq. 2.44), but also a longer precipitation duration (i.e the precipitation starts earlier, and ends later, at higher temperatures). The number of dispersoids at the end shows a high temperature dependence, with the volume fraction changing from 10^{20} at 350 °C, to 10^{15} at 450 °C. There is also a large reduction in the volume fraction of dispersoids, with almost 1.2 volume % dispersoids at 350 °C, to less than 0.02 volume % at 450 °C. This implies that the radius of the dispersoids has also been reduced.

Deformed material

In Figure 3.6b the Mn concentration in solid solution, and number and volume fraction of dispersoids, from Precipal simulations at different temperatures, from 350 to 450 °C for deformed material, is shown. The recrystallization kinetics used are based on experimental recrystallization curves from Lok[6], and are indicated by broken lines in the figure.

The overall trends are the same as for the undeformed material, (but shifted towards earlier precipitation), but with some additional interesting effects due to the introduced recrystallization course:

There is a large shift in the precipitation curves towards later precipitation when recrystallization occurs before the onset of precipitation (T = 450 and 420 °C). The precipitation course now shifts back to the same times as for the undeformed case. This is reasonable since the only difference between the simulations is fraction recrystallized, X, which now becomes the same (i.e 1) before any precipitation occurs.

When recrystallization occurs during precipitation (T = 410 °C) the precipitation stops for some time before it continues (i.e a step is introduced into the curves). The precipitation resumes when precipitation in undeformed material would have happened, and

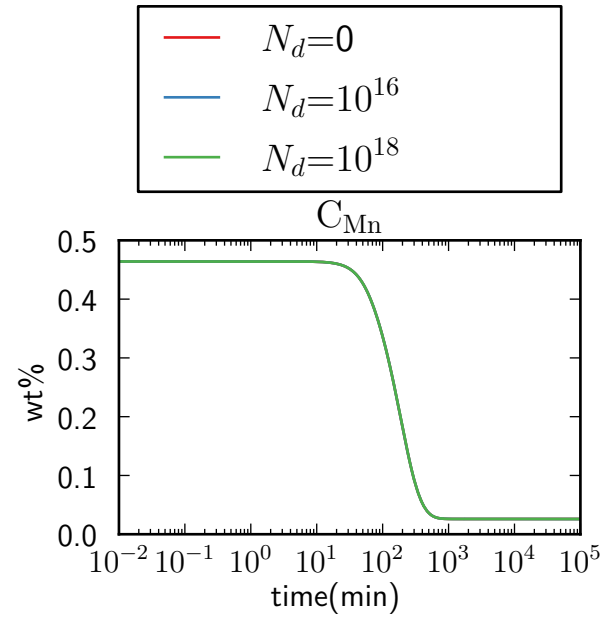

(a)

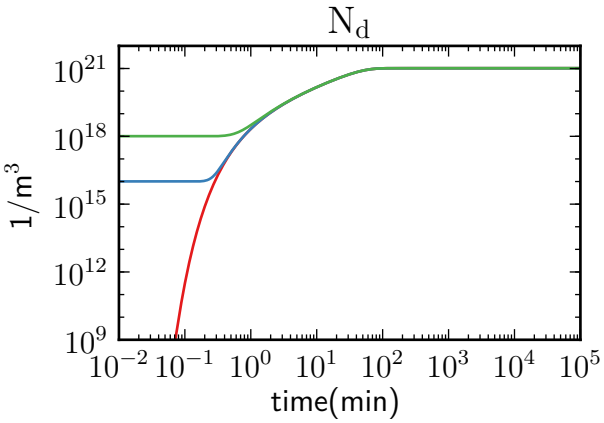

(b)

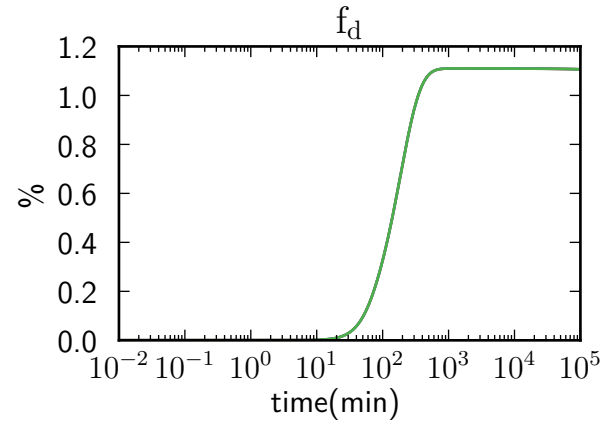

(c)

Figure 3.5.: A sensitivity study of the initial number of dispersoids, N_{d0}.

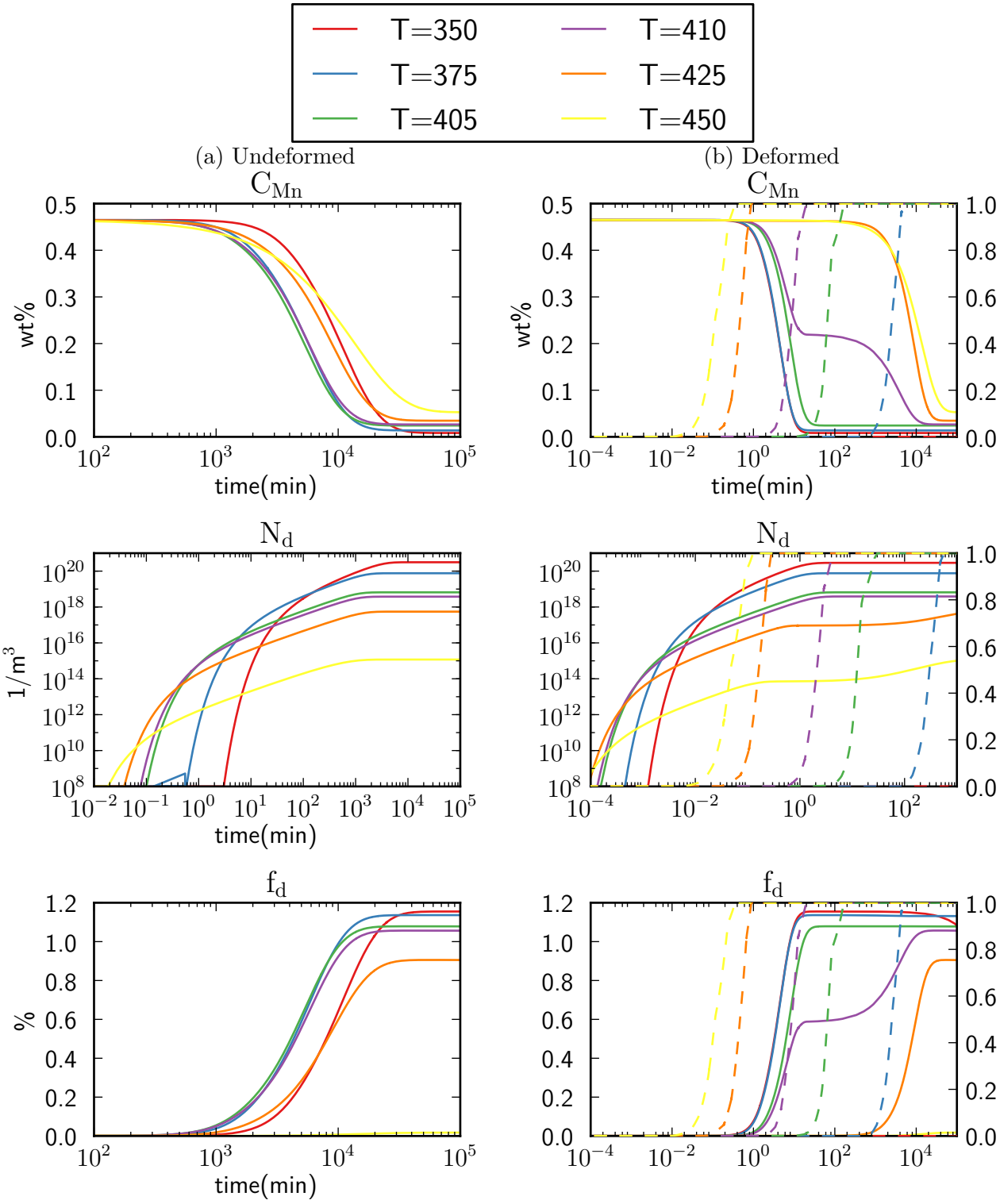

Figure 3.6.: Mn concentration in solid solution, the number of dispersoids, and volume fraction of dispersoids at different annealing temperatures for undeformed(left figures) and deformed (right figures) simulated with the physical precipitation model. The broken lines are fraction recrystallized.

follows the same precipitation course as the undeformed case during the rest of the annealing process.

3.4. Comparison of Precipal simulations with simulations by Lok

In this section simulation results from Precipal are compared with the simulation results presented in the doctoral thesis of Z. J. Lok[6]. Since the Fortran 77 version of Precipal, and thus also the Python implementation, are based on equations presented in this doctoral thesis, it was expected that the results presented would be reproduceable in Precipal, however this turned not to be the case.

Table 3.2 shows the input parameters used in the simulations presented by Lok in his thesis, and in the corresponding Precipal simulations. Lok states all concentrations in wt%, while the input for Precipal are in at%. It is unclear how Lok reached the concentrations in wt% that he states, because the values do not correspond with the stoichiometric compositions of the particles.

In Precipal on the other hand the Mn concentration in the dispersoids and constituents, C_d^p and C_c^p, are the stoichiometric concentrations. Therefore these values do not correspond with the values used by Lok. The prefactor for the equilibrium solubility of Mn in solid solution, C^s (Eq. 2.44), is based on the value used by Lok (named $C_{0,\mathrm{Mn}}$ in Lok), but converted into at% based on the nominal alloy composition.

Table 3.2.: Input parameters used in Figure 5.4 from Table 5.2 in Lok[6, p. 90-91], and corresponding values used in Precipal. Parameters with different units are colored red.

parameter	**Lok**		**Precipal**	
δ_{SGB}	4.0496×10^{-10}	m	4.0496×10^{-10}	m
σ	0.324	Jm^{-2}	0.324	Jm^{-2}
ν_{Al}	1.66026×10^{-10}	m^{-3}	1.66026×10^{-10}	m^{-3}
a_0	4.0496×10^{-10}	m	4.0496×10^{-10}	m
C_d^p	42.37	wt%	18.75	at%
C_c^p	28.83	wt%	14.286	at%
C^s	7.716×10^{3}	wt%	3821	at%
$D_{0,\mathrm{Mn}}^L$	1.04×10^{-2}	$\mathrm{m}^2\mathrm{s}^{-1}$	1.04×10^{-2}	$\mathrm{m}^2\mathrm{s}^{-1}$
N_c	6.87×10^{15}	m^{-3}	6.87×10^{15}	m^{-3}
r_c	1.1211×10^{-6}	m	1.1211×10^{-6}	m
$Q_{c,\mathrm{Mn}}$	7.15×10^{-4}	Jmol^{-1}	7.15×10^{-4}	Jmol^{-1}
$Q_{D,\mathrm{Mn}}^L$	2.109×10^{5}	Jmol^{-1}	2.109×10^{5}	Jmol^{-1}
V_m^α	9.68×10^{-6}	$\mathrm{m}^3\mathrm{mol}^{-1}$	9.68×10^{-6}	$\mathrm{m}^3\mathrm{mol}^{-1}$

3.4.1. Physical Model

In this section simulations performed with the physical precipitation model is compared with the simulation results presented in Lok[6]. The most relevant input parameters are

presented in Table 3.2, while the remaining parameters can be found in Appendix C.

Undeformed material with normal nucleation

This is the most basic case with the fraction recrystallized, set to one ($X = 1$, the reference case). This input corresponds with the simulations presented in Figure 5.4 (a) in Lok[6, p. 91].

Figure 3.7a compares the Mn concentration in solid solution, number density of dispersoids and volume fraction of dispersoids, simulated with the physical precipitation model, with relevant simulations performed by Lok.

The initial and final Mn concentration coincides with Lok's results, but the reaction starts later with Precipal .

The difference in the number of dispersoids is more pronounced. The final number of dispersoids from Precipal is about four orders of magnitude lower than the results of Lok. It should be stated that Lok does not state the initial number of dispersoids, but it is assumed to be zero. Precipal was run with different number of initial dispersoids, but there was no difference in the final number of dispersoids (see Sec 3.3.4). As for the Mn concentration, it can also here be seen that the reaction starts later in Precipal.

The final volume fraction of dispersoids is about half the amount with Precipal compared to Lok's results. It can also here be seen that the reaction starts later in Precipal.

Simulations with different values for the parameters converted from wt% to at% were performed, for instance with the conversion based on nominal alloy composition, and simulations with all parameters in wt% (i.e no conversion of the parameters), but none of this gave results that coincided more closely with Lok's results than the results presented here. The cause of the discrepancy between Precipal simulations, and the results by Lok has unfortunately not been identified. However with confidence in the Precipal implementation and the present choice of input parameters the simulation work was continued.

Undeformed material with site-saturation nucleation

In this case the input parameters are the same as for the undeformed material except that site-saturation nucleation is used, which means that the number of dispersoids is set to zero in the beginning, and after an incubation time, all dispersoids nucleate simultaneously. In this case the incubation time is 300 min, and the number density of dispersoids is 2.74×10^{17} $1/m^3$. These input parameters corresponds to the ones used in Figure 5.4 (b) in Lok[6, p. 91].

Figure 3.7b compares Mn Concentration in solid solution, number density of dispersoids and volume fraction of dispersoids, respectively, from Precipal simulations, and the results from Lok's thesis. The short simulation time presented (i.e equilibrium is not achieved) is due to Lok only presenting results for the time span shown here.

The solid solution concentration and number of dispersoids coincides well with Lok's simulations. The small discrepancies between the curves in the N_d plots is most likely due to small errors introduced from copying the results from Lok's figures. The volume fraction of dispersoids starts out similarly (at $f_d = 0$), but strongly deviates as the simulation continue.

Deformed material with normal nucleation

Here the input parameters used are the same as for the undeformed case, with the exception of volume fraction recrystallized (X) which is now set to values following an experimental recrystallization curve by Lok[6]. The results form this simulation are shown in Figure 3.8a. In contrast to the undeformed case the precipitation simulated by Precipal occurs earlier, and the final number of dispersoids are higher, than in Lok's simulations. The difference in volume fraction of dispersoids on the other hand are about the same.

The solid solution concentration is more dependent on the fraction recrystallized in Precipal, with the C_{ss} shifting about 100 min for Precipal, while for Lok the shift is about 10 min (both towards earlier precipitation).

The final number of dispersoids in Precipal is unchanged compared with the undeformed simulations, while for Lok's simulations the final number of dispersoids drops from about 6×10^{22} to 2.4×10^{20} $1/m^3$.

The volume fraction of dispersoids are unchanged between the undeformed and deformed case both for Precipal simulations, and for the Lok's simulations.

Deformed material with site-saturation nucleation

Here the same input parameters as for the undeformed case with site-saturation nucleation is used, except that recrystallization is introduced, based on experimental recrystallization curves by Lok[6]. Figure 3.8b shows the results from these simulations. The degree of consistency between Lok and Precipal is the same as in the undeformed case, with solid solution concentration and number of dispersoids being consistent, while the volume fraction of dispersoids deviates,

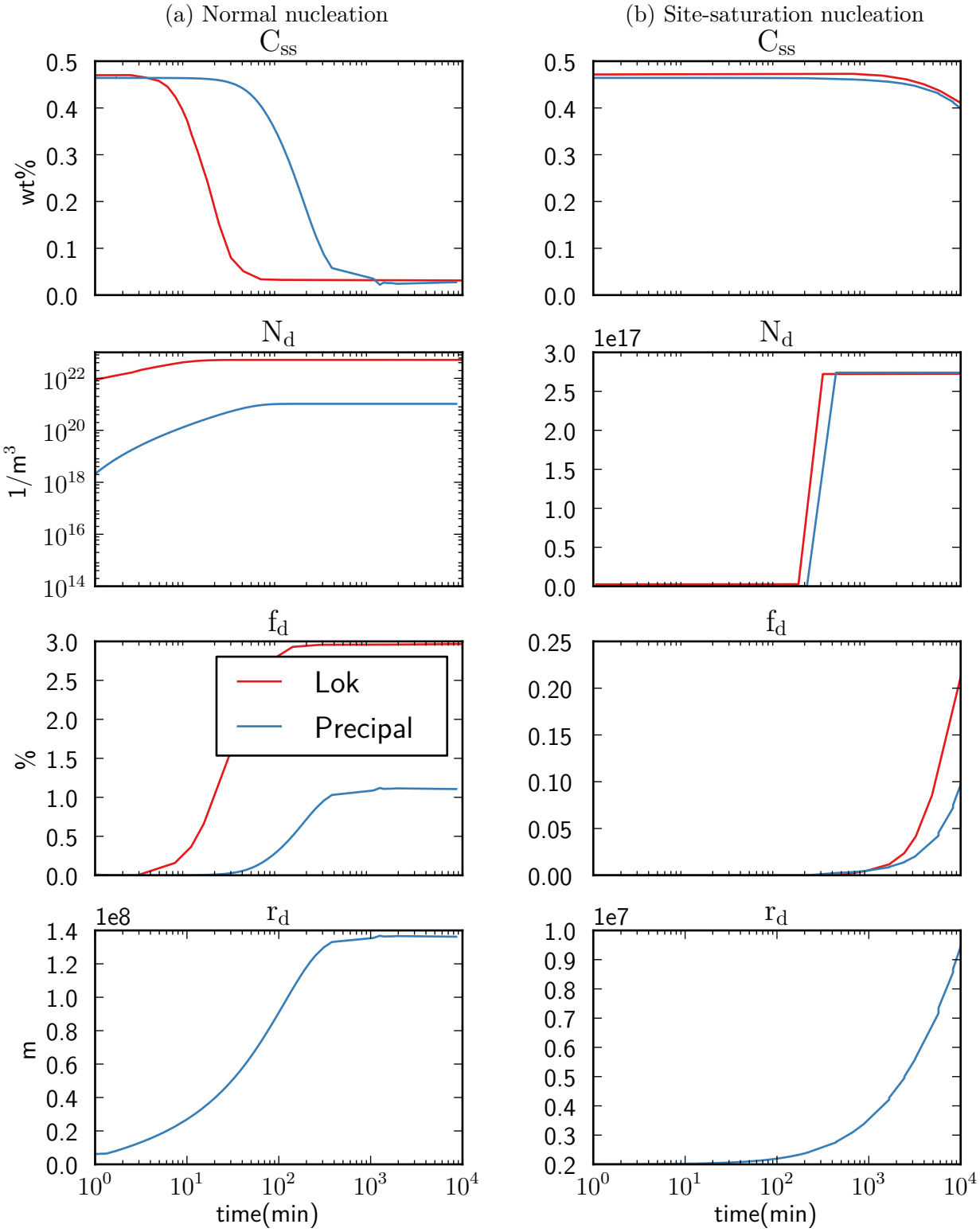

Figure 3.7.: Comparison between simulations from Precipal at 405°C of an undeformed material and the results presented in the doctoral thesis of Z. J. Lok[6, p. 91]. The incubation time for site-saturation nucleation is 300 min, and the number of dispersoids is 2.74×10^{17} $1/m^3$.

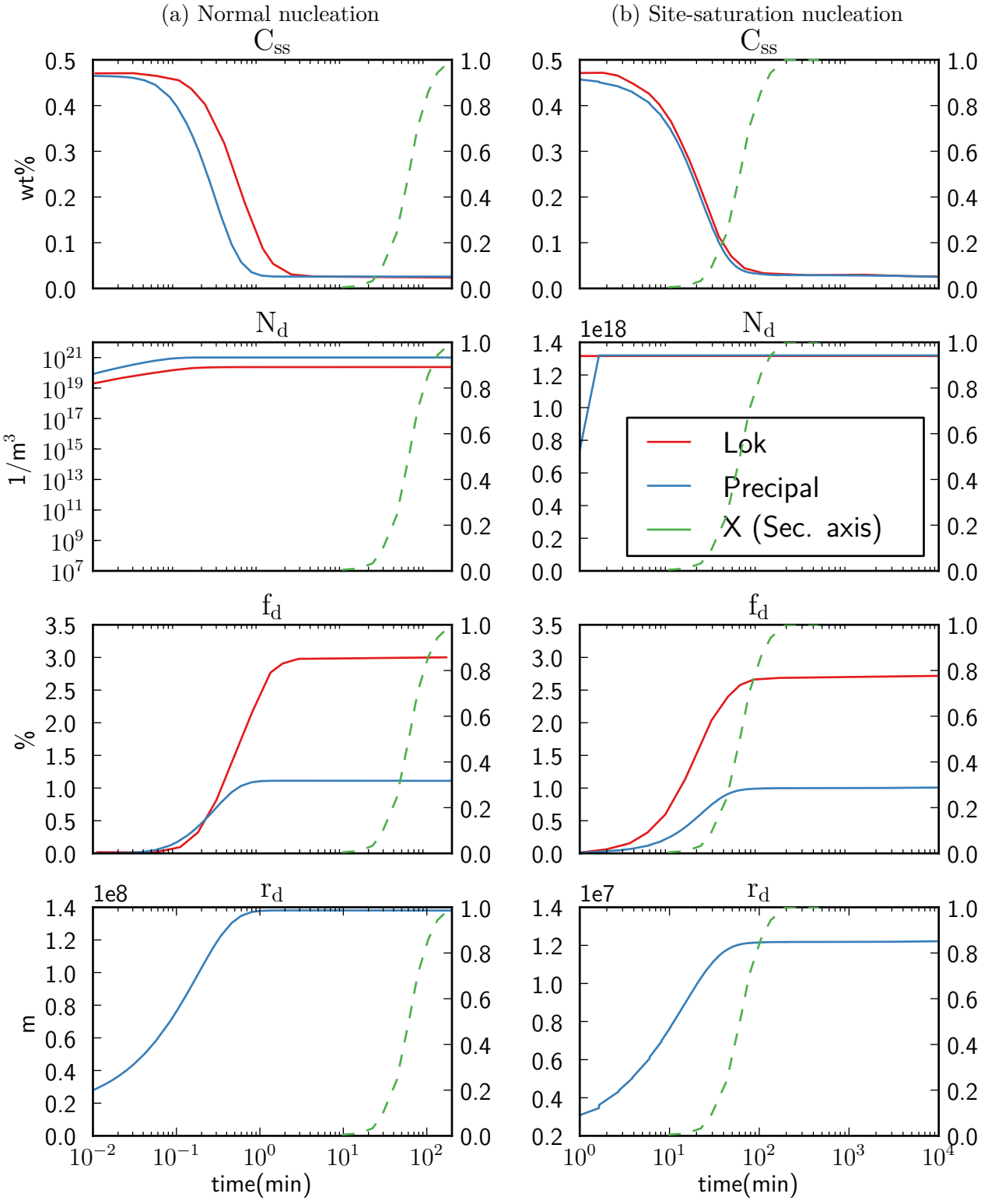

Figure 3.8.: Comparison between simulations from Precipal at 405°C of an deformed material and the results presented in Figure 5.4 (c) (left figures) and (d) (right figures) in the doctoral thesis of Z. J. Lok[6, p. 91]. The incubation time for site-saturation nucleation is 1 min, and the number of dispersoids are 1.32×10^{18}.

3.4.2. Phenomenological Model

The principles of the phenomenological model, and the motivation for its introduction are explained in Section 2.5.5. Here nucleation of dispersoids is simplified as site-saturation nucleation, with no incubation time (i.e all nucleation at $t = 0$). The number of dispersoids is thus constant, and is provided as an input parameter based on experimental data from Lok[6]. The number of dispersoids at different temperatures can be observed in Table 3.3.

The parameters where fitted to the same experimental data as in Lok[6], but since Precipal uses atomic fraction instead of weight percent as concentration units, the actual values of the fitting parameters used are different, as shown in Table 3.4.

Undeformed material

The undeformed material is assumed to be completely recrystallized, i.e $X = 1$. The fitting was performed against the same experimental data at the same temperatures as done by Lok (volume fraction of dispersoids and solid solution concentration at 375 and 405 °C), and compared with experimental data at 405 °C due to this being the only temperature (other than the fitting temperatures) with experimental data for volume fraction of dispersoids.

Results from phenomenological Precipal simulations for the undeformed reference material is shown in Figure 3.9. Here the markers represents experimental data, with the fitting done against the square markers. The simulated results match the experimental data well, except for the volume fraction of dispersoids at 405 °C, which is underestimated by the simulation. This is the same results as obtained by Lok's precipitation model [6, chap. 5.4].

Deformed material

The deformed material uses experimental recrystallization data as an external input parameter[6]. The fitting was also here done against the same variables at the same temperatures as done by Lok; Volume fraction of dispersoids and solid solution concentration, at 405 °C. Note that here the fitting is done at only one temperature.

Results from the phenomenological Precipal simulations for the deformed material can be observed in Figure 3.10. The solid solution concentration curve nicely follows the experimental data at 405 °C, also at the unfitted data points. The volume fraction of dispersoids on the other hand fails to match the experimental data at the unfitted data point. At 425 °C the simulated solid solution concentration match the experimental data, while the volume fraction of dispersoids is underestimated. At 375 °C the solid solution starts to drop too early (i.e precipitation starts to early). This can also be seen in the

Table 3.3.: Number of dispersoids and initial dispersoid radius used in the phenomenological model.

Temperature(°C)	N_d $(1/N^d)$	r_{d0}(nm)
375	7.18×10^{17}	12.9
405	2.74×10^{17}	20.0
425	1.46×10^{17}	25.0

Table 3.4.: Fitting parameters used in the Phenomenological model. The superscript d and c means *deformed* and *undeformed*, respectively. The subscripts d and c means *dispersoids* and *constituents*, respectively.

Parameter	Lok		Precipal	
n	6		6	
$\theta_d^u(N_d)$	$55.7N_d^{-0.467}$	wt%$^{\frac{1}{5}}$m	$3.6704N_d^{-0.467}$	(at. frac.)$^{\frac{1}{5}}$m
θ_d^d	1.9×10^{-7}	wt%$^{\frac{1}{5}}$m	2.7790×10^{-8}	(at. frac.)$^{\frac{1}{5}}$m
$\theta_c^u(T)$	$3.24\times10^{-9}\exp\left(\frac{5.470\times10^3}{T}\right)$	wt%$^{\frac{1}{5}}$m	$2.1350\times10^{-10}\exp\left(\frac{5.470\times10^3}{T}\right)$	(at. frac.)$^{\frac{1}{5}}$m
θ_c^d	3×10^{-6}	wt%$^{\frac{1}{5}}$m	1.3970×10^{-7}	(at. frac.)$^{\frac{1}{5}}$m

volume fraction of dispersoids, which in addition to starting to rise too early, also becomes much higher than the experimental value.

The simulated Precipal results are the same as the results obtained by Lok in his simulations[6, chap 5.4] (i.e with the same shortcomings as Precipal).

3.5. Coupling of Precipal and Alsoft

In this section results from Alsoft simulations and results from the coupling between Alsoft and Precipal (as described in Section 2.6) will be presented.

The input parameters used by Precipal are the same as in Section 3.4.1 and 3.4.2 for the physical and phenomenological model, respectively.

The input used by Alsoft are based on the input used by Wang [24], which are based on experimental data from almost the same alloy as the one used by Lok (Al-1Mn-0.5Fe-0.1Si in Wang, Al-1.1Mn-0.51Fe-0.06Si in Lok). The pre-annealing treatment (in terms of i.e cold rolling) is different between Wang and Lok. The material used by Wang is deformed to a strain of 3, while the material used by Lok is deformed to a strain of 2. In order to be more consistent with the experimental data from Lok (on which the Precipal input is based) the initial subgrain size was changed to 1 μ m, and the simulated grain size and recrystallization kinetics was fitted to experimental data, as explained in the next section. The standard input used can be observed in Appendix C.2.

3.5.1. Fitting of grain size and recrystallization kinetics to experimental data

The grain size simulated by Alsoft was fitted to the experimental grain size data at T=450 °C shown in Figure 3.11a (i.e a condition assumed to be unaffected by precipitation). The experimental grain size was calculated by dividing the length of the lines by the number of grains crossed by the lines. The results from this are shown in Table 3.5. It must be noted that the calculated grain size is not very accurate, as the resolution of the image is poor.

The simulated grain size was fitted by adjusting the constants in the expressions for the number of nucleation sites (Eq. 2.10, 2.11 and 2.16), C_{PSN}, C_{Cube} and C_{GB}. The parameters were selected so that the relative amounts of each nucleation site type was

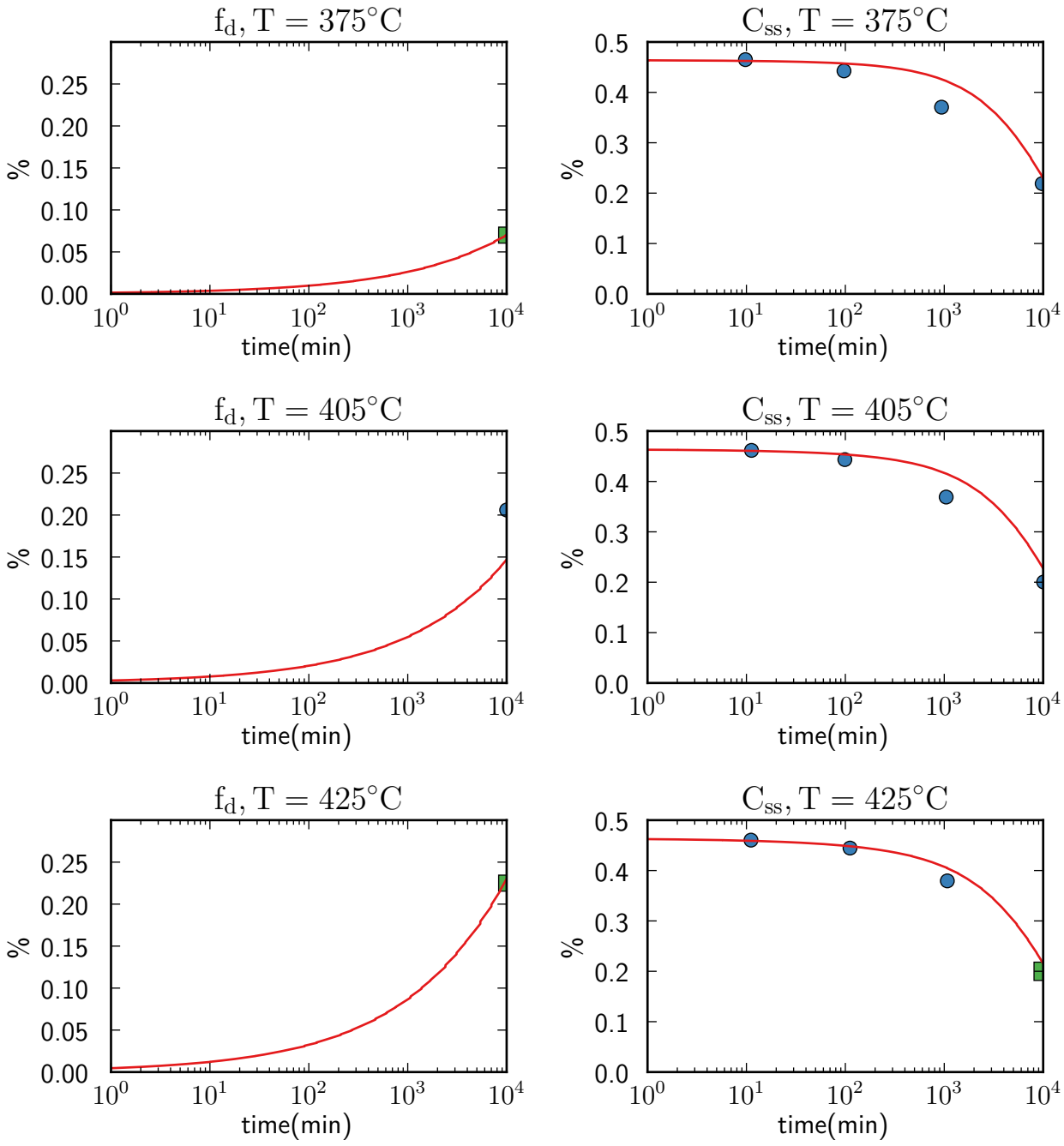

Figure 3.9.: Volume fraction of dispersoids and Mn concentration in solid solution at different temperatures. The lines are from phenomenological Precipal simulations of an undeformed sample (i.e $X = 1$), while the dots are experimental data from Lok[6].

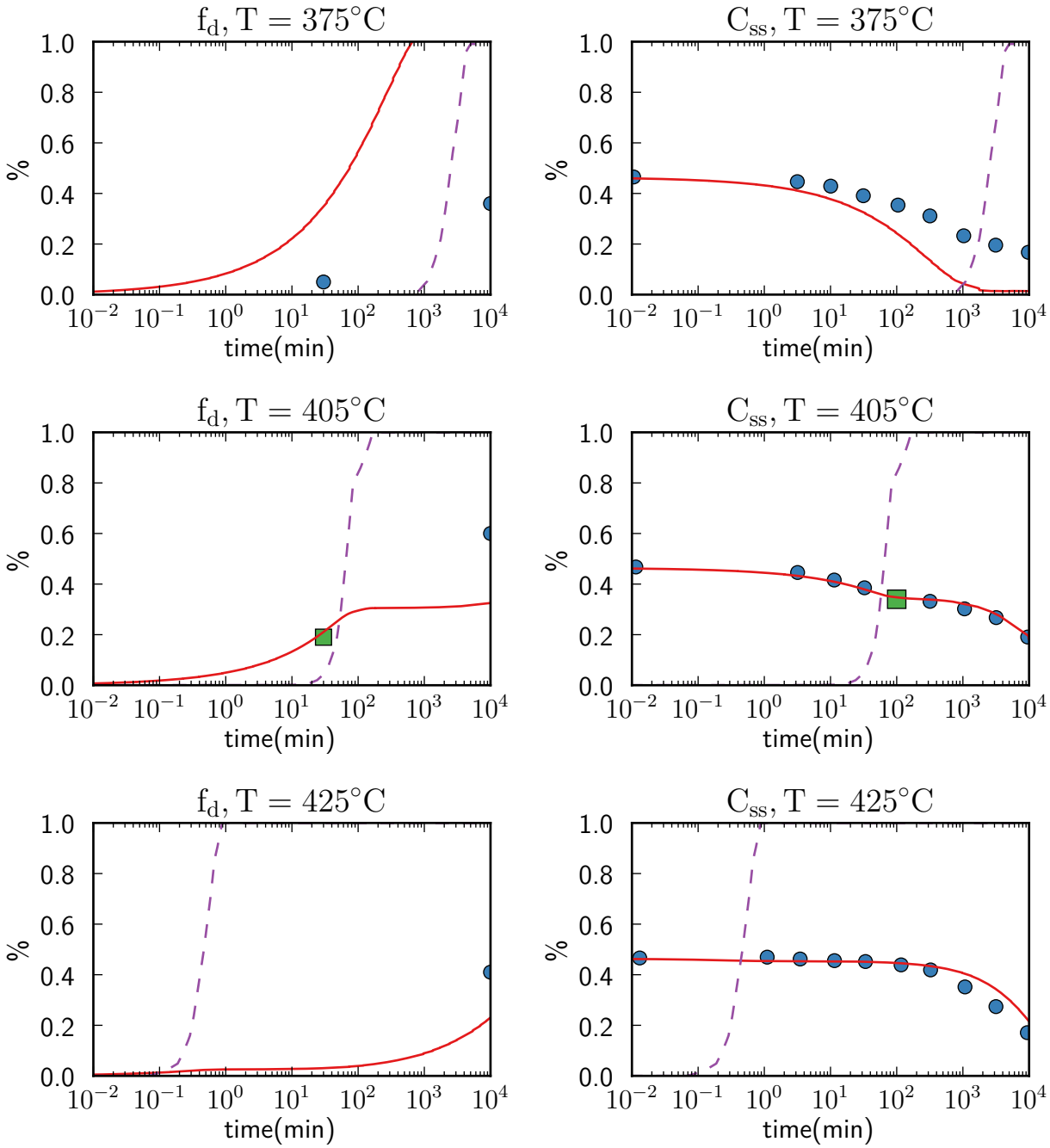

Figure 3.10.: Volume fraction of dispersoids and Mn concentration in solid solution at different temperatures. The solid lines are from phenomenological Precipal simulations of an deformed sample (with recrystallization kinetics as input), while the markers are experimental data from Lok[6]. The broken lines are fraction recrystallized. The simulations are fitted against the square markers.

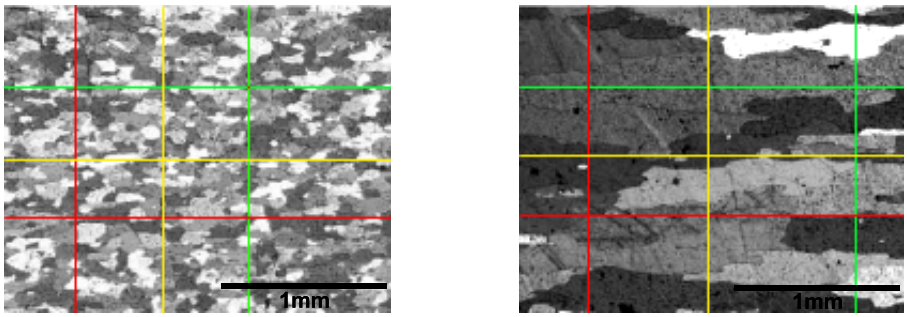

(a) T=450 °C (b) T=405 °C

Figure 3.11.: The recrystallized grain structure after annealing [6]. The grains where counted along the indicated lines.

Table 3.5.: Number of grains along the lines in Figure 3.11, and the corresponding grain size.

		green	red	yellow	Grain Size (μm)
T=450	# grains along vertical line	26	25	21	74
	# grains along horizontal line	18	12	19	133
	average				103
T=405	# grains along vertical line	14	9	10	162
	# grains along horizontal line	2	3	3	813
	average				487

unchanged. The parameters found to reproduce the experimental grain size at 450 °C are: $C_{PSN} = 0.0247$, $C_{GB} = 5.0699 \times 10^{-3}$ and $C_{cube} = 85.517$.

The simulations were also fitted to an experimental recrystallization curve at 450 °C [6, p.59]. This was achieved by tuning the mobility for the growth rate of recrystallized grains, by changing the prefactor in the expression for the mobility, M_0 (see Sec. 2.4.4, Eq. 2.21). The mobility prefactor found to correspond with the experimental data was $M_0 = 10^5$ m^4/s (consistent with what was also used by Wang [11]).

3.5.2. Recrystallization kinetics

Figure 3.12 shows fraction recrystallized at different temperatures for uncoupled Alsoft simulations, and Alsoft coupled with the physical and phenomenological precipitation model, together with experimental data from Lok[6].

The uncoupled Alsoft simulations shown in Figure 3.12a corresponds well with the experimental data at T=450 °C and T=425 °C, but the correlation decreases with decreasing temperature. The uncoupled simulated recrystallization curves are too fast at lower temperatures.

The Alsoft simulations coupled with the physical precipitation model (Fig. 3.12b) are at T=450 °C and T=450 °C displaced some towards faster recrystallization times compared with the uncoupled simulations. The only parameters that are different in the recrystallization model during the coupling are the Zener-drag and the solid solution concentration. For the uncoupled case the Zener-drag is zero for the entire recrystallization

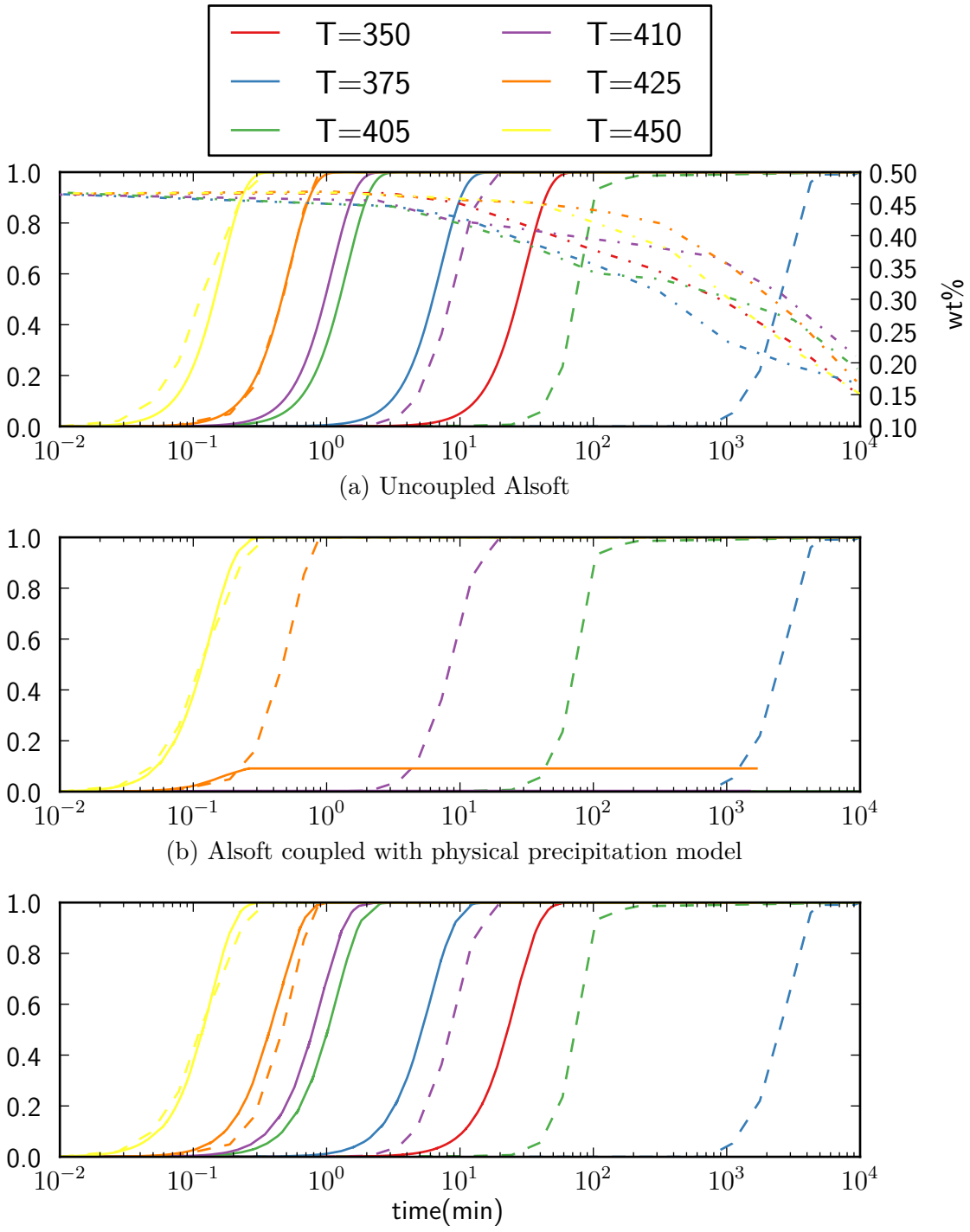

(a) Uncoupled Alsoft

(b) Alsoft coupled with physical precipitation model

(c) Alsoft coupled with phenomenological precipitation model

Figure 3.12.: Fraction recrystallized at different temperatures. The solid lines are from Alsoft and Alprec simulations, while the dashed lines are experimental recrystallization curves and the dash-dotted lines are experimental solid solution concentrations[6].

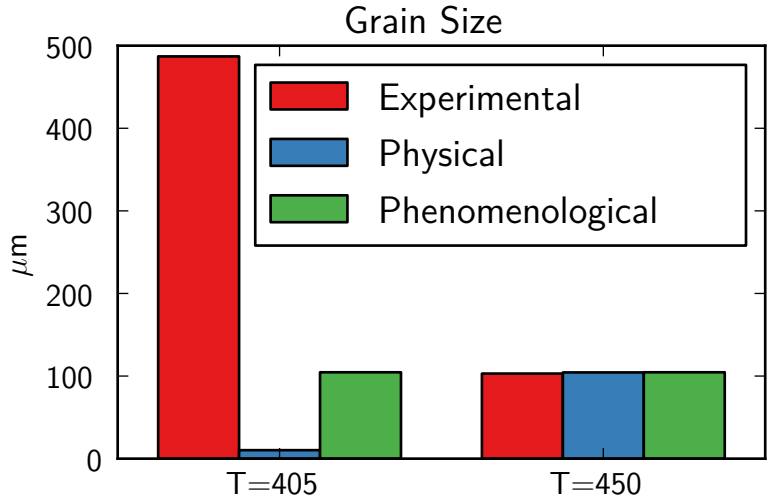

Figure 3.13.: Simulated Grain size at the end of the simulations, and experimental grain size from Lok[6].

.

duration, while in the coupled case the Zener-drag starts out with a small contribution from the constituent particles, before later receiving a larger contribution from the dispersoids. This would move the recrystallization curve in the other direction (i.e towards later recrystallization) compared with the uncoupled case, so the difference in Zener-drag is clearly not the reason for the shift in the recrystallization curve. The solid solution concentration is constant at 0.97 % for the uncoupled case, while for the coupled case it starts out at 0.47 % before dropping when precipitation starts. This is the cause of the shift in the recrystallization curve towards earlier precipitation during the coupling, as lower solid solution concentration leads to a higher mobility of the boundary of a growing recrystallized grain, and thus earlier recrystallization (see Sec. 2.4.4, and Eq. 2.21).

At T=425 °C the recrystallization is stopped after about 10% recrystallized. At lower temperatures there are no recrystallization.

The recrystallization curves from Alsoft coupled with the phenomenological model (Fig. 3.12c) are very similar to the uncoupled case for all temperatures, but in this case shifted somewhat towards faster recrystallization. The reason for this being the same as for the simulations coupled with the physical precipitation model.

Overall, the coupling of Alsoft with Precipal has limited effect on the simulated recrystallization kinetics, except when the recrystallization is halted completely by the Zener-drag.

3.5.3. Grain size

Figure 3.13 shows the grain size at the end of the simulations together with experimental grain sizes. There are no change in the simulated grain size between the different precipitation models, or at different temperatures, except for the physical case at T=405 °C. This case was not completely recrystallized (Fig. 3.12b), and because the Alsoft model uses site-saturation nucleation (all nucleation occurs at t=0), the number of grains is the same as at the other temperatures, while the recrystallized volume fraction is smaller,

resulting in smaller grains (ref. Eq. 2.9). Site saturation nucleation is also the reason for the lacking temperature dependence in the simulated grain sizes, as all nucleation occurs at t=0, before annealing commences, and is determined by the deformed state alone.

An initial Zener-drag caused by constituent particles have in principle an effect on the number of nucleation sites (Eq. 2.10, 2.11 and 2.16), but due to the large size of the constituent particles the contribution is negligible.

3.5.4. Comparison with experimental data

Figure 3.14 shows simulated and experimental fraction recrystallized and solid solution concentrations, as well as the Zener drag, at T=405 °C and T=450 °C for uncoupled Alsoft simulations, and Alsoft simulations coupled with the physical and phenomenological precipitation model.

For the uncoupled cases the Zener drag and solid solution concentration are constant, as they are given as external parameters.

In the cases coupled with the physical precipitation model the precipitation starts too early compared with the experimental data. This can be seen both at T=405 °C and T=450 °C. It can also be observed that after precipitation starts, the precipitation is too fast and abrupt, compared with the experimental data. In the physical case there are no recrystallization at T=405 °C, this can be explained by the high Zener drag (approx. 0.4 MPa after 1 minute) before recrystallization gets a chance to start. The Zener drag starts at a low value, with the constituent particles as the principal contributor, but after precipitation starts the Zener drag quickly rises to a much higher value caused by the precipitates.

When the precipitation occurs before recrystallization (as in the physical case at T=405 °C), the precipitation can have a restraining effect on the recrystallization, but often the simulated recrystallization kinetics are so fast that the material is fully recrystallized before the onset of precipitation (as in the physical case at T=450 °C). The initial Zener-drag caused by the constituents are too small to have a significant impact on the recrystallization kinetics.

In the cases coupled with the phenomenological precipitation model the solid solution concentration follows the experimental data. The simulated Zener drag is much lower than in the physical case, so in this case the material is fully recrystallized at T=405 °C.

Precipitation

Figure 3.15 shows radius, volume fraction and number density of dispersoids and constituents at T= 405 and 450 °C for Alsoft simulations coupled with the physical and phenomenological precipitation model.

The radius of the dispersoids and constituent are generally larger in the phenomenological cases. The volume fraction of dispersoids are larger in the physical model simulations, while for the constituents this is reversed, with the volume fractions larger for the phenomenological simulations compared with the physical simulations. The number of dispersoids are higher in the physical model simulations compared with the phenomenological model simulations. This is the reason for the for the lower Zener-drag in the phenomenological model simulations (as discussed in Sec. 3.5.4), as lower amount of larger particles results in a lower Zener-drag (Eq. 2.2).

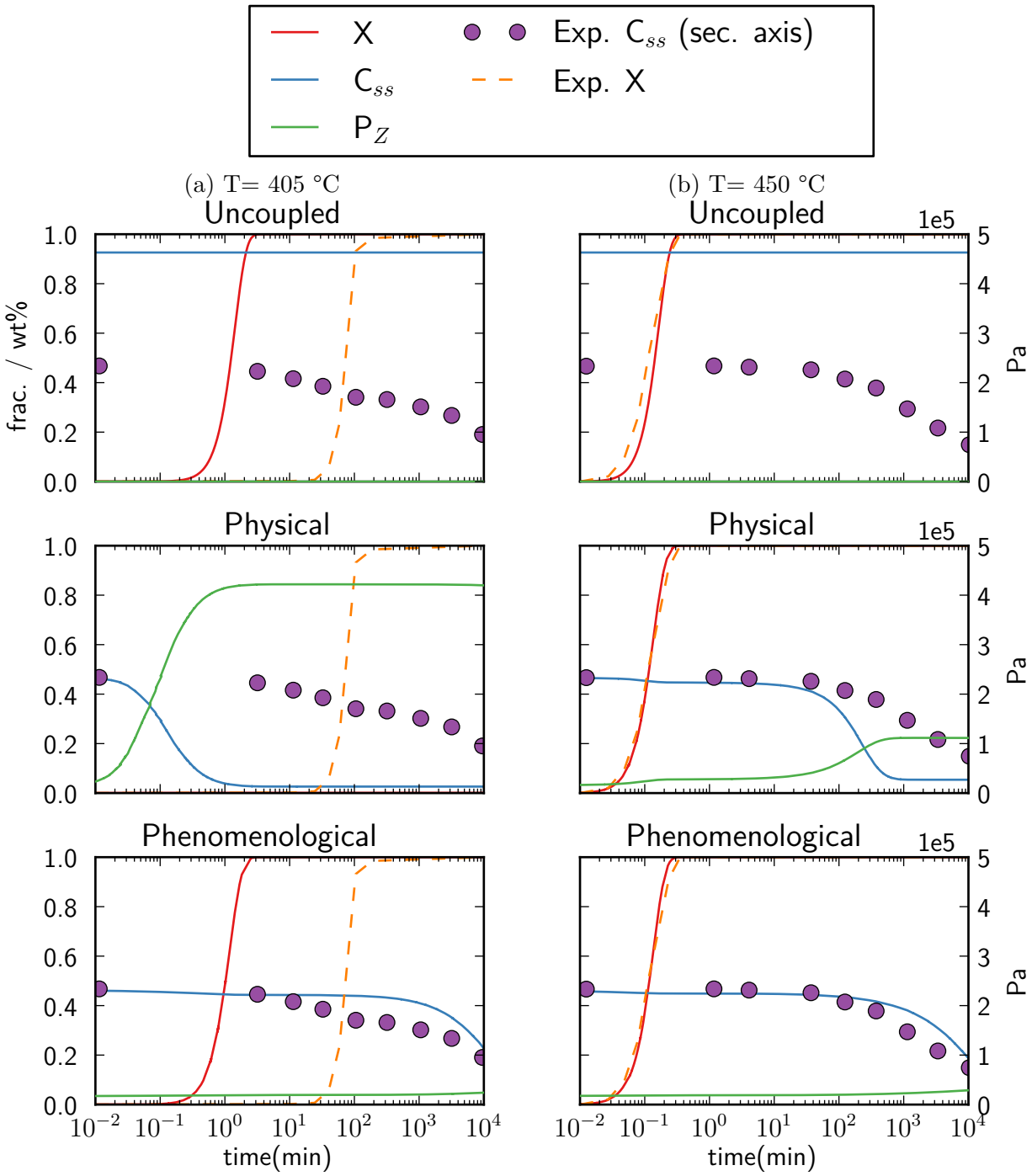

Figure 3.14.: Simulated and experimental fraction recrystallized and effective solid solution concentration, and simulated Zener drag at T=405 °C (left figures), and T=450 °C (right figures). Experimental data from [6].

For the physical model simulations the radius of the dispersoids are lower at T=405 °C than at T=450 °C. This is reversed for the volume fraction of dispersoids, where the highest values are found at t=405 °C. Since the radius is larger, and the volume fraction lower at 450 °C the number of dispersoids also has to be lower at 450 °C compared with 405 °C. For the phenomenological model simulations both the radius and volume fraction of dispersoids are lower at T=405°C, and the number of dispersoids are the same at both temperatures (due to site saturation nucleation).

For the constituents, both the radius and the volume fraction are larger at T=405 °C, and the number of constituents are of course the same for all simulations, as this is given as an input parameter and treated as a constant.

3.5.5. Artificial Zener drag

The coupling between the recovery and recrystallization model, Alsoft, and the precipitation model, Precipal, failed to reproduce the experimental data from Lok[6]. The simulated recrystallization still starts too early, as shown in Section 3.5.2. One reason for this discrepancy could that the effects of the Zener drag on nucleation is underestimated by the current recrystallization nucleation model. With site-saturation nucleation of recrystallization the effect of all precipitation taking place after $t = 0$ (i.e concurrent precipitation) is completely neglected.

In order to find out how much "extra" Zener-drag is required to reproduce the experimental recrystallization curves the recrystallization curve was first fitted at T=450 °C (with the mobility prefactor, as explained in Sec. 3.5.1), before the temperature was changed to 405 °C, and an extra Zener-drag was added (as explained in Appendix B.2), until the simulated recrystallization curve reproduced the experimental curve.

The results from these simulations are shown in Figure 3.17. When there is no extra Zener-drag at T=405 °C the simulated recrystallization curve is, as expected, to fast. When it is increased to 100 kPa the material will not recrystallize fully because of the high Zener-drag. In order to be able to increase the Zener-drag during nucleation, and still have recrystallization the Zener-drag was set to Zero after the onset of recrystallization (i.e only Zener-drag during nucleation), as explained in Appendix B.2. When the artificial Zener-drag was set to 230 kPa the simulated recrystallization curve matches the experimental curve. If the Zener-drag is set even higher the recrystallization will become slower than the experimental.

Final grain size for the same simulations are shown in Figure 3.16. The artificial Zener-drag up to 100 kPa has negligible effect on the grain size. With an extra Zener-drag of 230 and 250 kPa the grain size increases dramatically, to about 2 and 5 mm, respectively. The reason for this dramatical increase can be seen in the equations for the number of nucleation sites (Eq. 2.10, 2.11 and 2.16). When the Zener-drag (P_Z) approaches the driving force for recrystallization (P_D), the number of recrystallization sites dramatically decreases, and accordingly the grain size will increase.

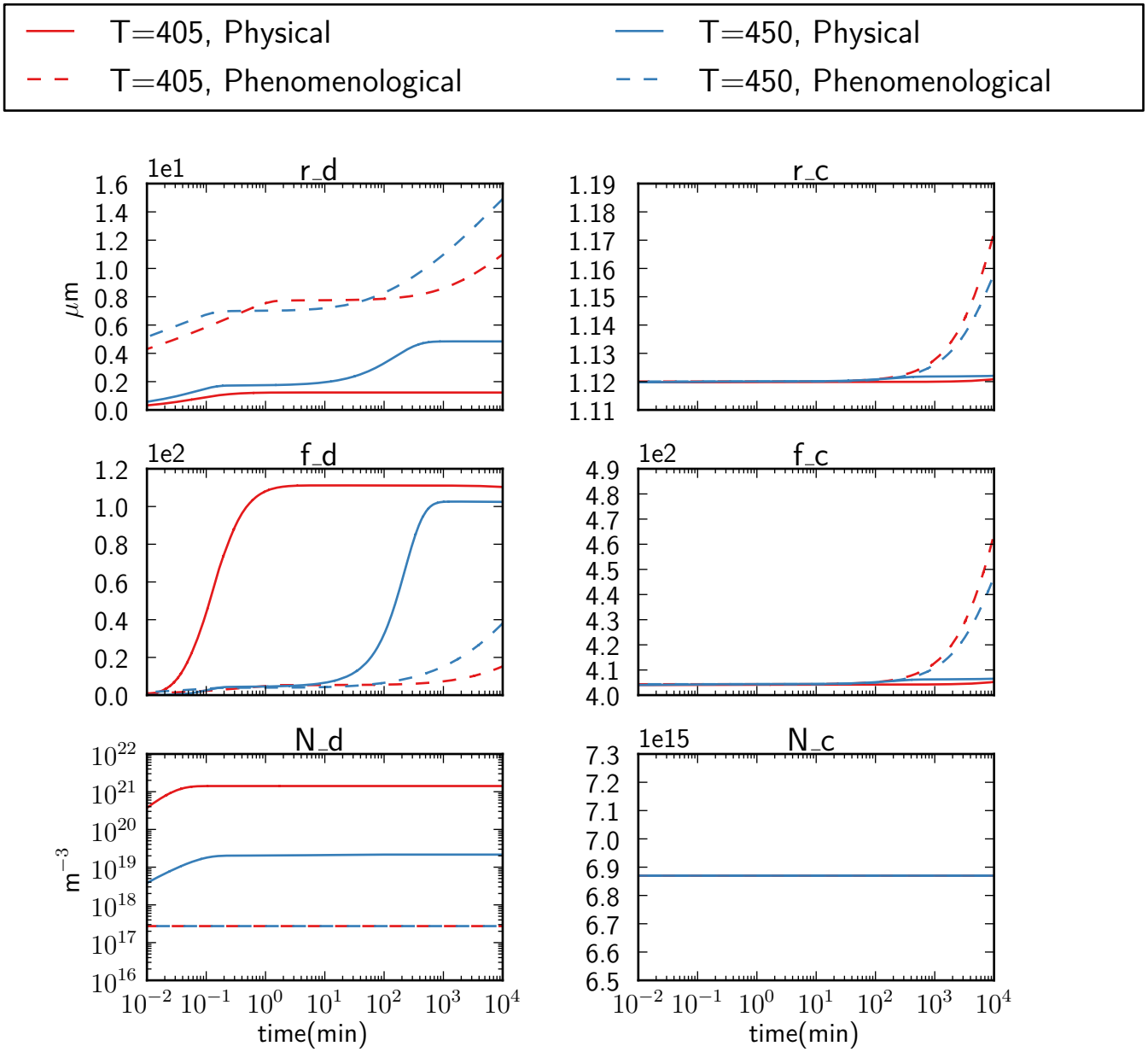

Figure 3.15.: Radius, volume fraction and number density of dispersoids and constituents at T=405 °and T=450 °C for Alsoft simulations coupled with the physical and phenomenological precipitation model. The number of constituents are the same for all simulations.

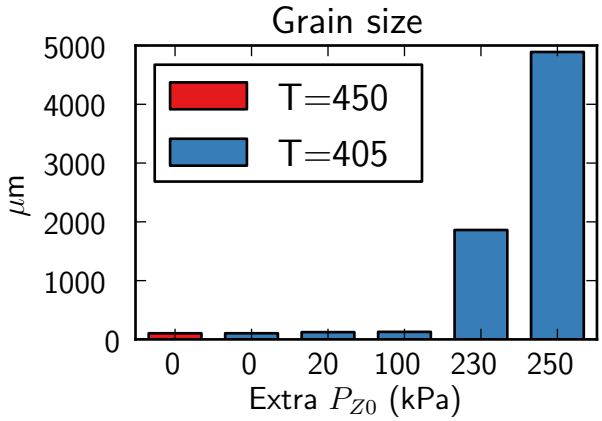

Figure 3.16.: Simulated Grain size at the end of the simulations for simulations with different artificial Zener-drag.

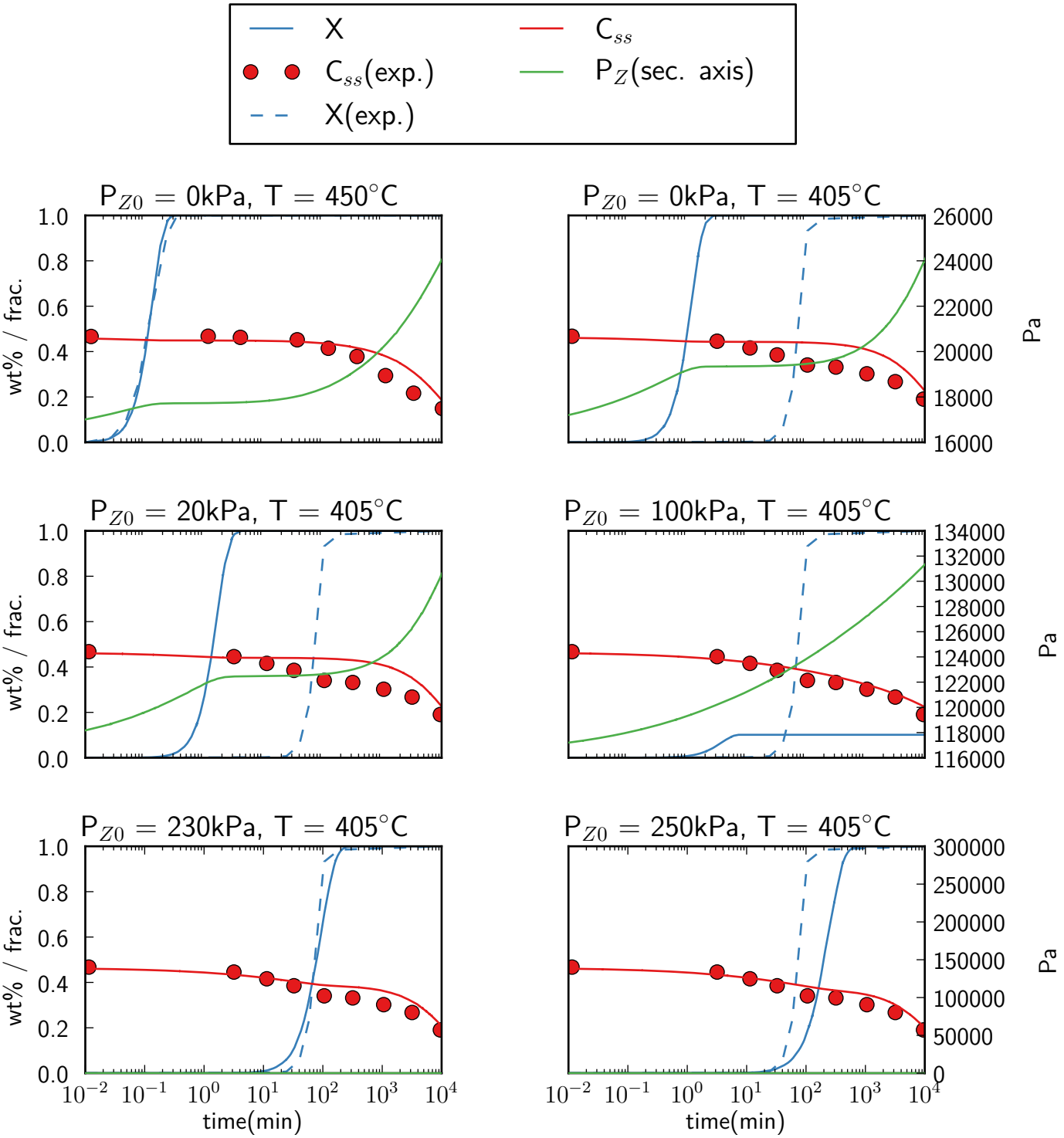

Figure 3.17.: Fraction recrystallized and solid solution concentration from coupled simulations and experimental data[6], and simulated Zener-drag. P_{Z0} is an extra external Zener drag. For the simulations with P_{Z0} = 230 and 250 kPa the Zener drag was set to zero after the onset of recrystallization.

4. Discussion

4.1. Implementation

In this section the challenges met during the reimplementation of Precipal in Python, and the coupling of Precipal and Alsoft, will be discussed. All comments about performance are based on simulations run with Python 2.7.5 in 64-bit Windows 8 on an Intel i5-2430M processor clocked at 2.4 GHz with 4 GB RAM.

4.1.1. Reimplementation of Precipal in Python

The reimplementation of Precipal in Python was carried out successfully, with only minor changes to the original precipitation model implemented in Fortran 77. The new implementation produce the same results as the old implementation, this implies that all validation done to the previous model should also be valid for the new implementation.

There are existing code libraries to facilitate interaction between Python and Fortran code (e.g F2PY[25]), however the use of these libraries can often be cumbersome, and the interaction between the programs would become more complex. The way the Python version of Precipal is implemented makes it easy to couple it with Alsoft, as both programs are structured in the same way, i.e they are both basically a set of differential equations, and uses the same format in their respective input and output files.

One downside of the Python implementation compared with the Fortran 77 implementation could be speed, well optimized Fortran code are generally faster than corresponding Python code[26]. This problem is partially avoided by the use of the *odeint* integrator from the Python library *scipy.integrate*, which is a wrapper around the differential equation solver *lsoda* from the Fortran library *odepack*, i.e the most performance sensitive part of the code is still basically Fortran code. Langtangen et.al[26] shows that Python code with loops implemented in Fortran (i.e the solving of the differential equations) obtain the same performance as pure Fortran code.

For all the uncoupled Precipal simulations performed in this thesis performance was not a big issue. All simulations used a reasonable amount of computing time (less than five minutes at most, majority of simulations took less than 30 seconds).

4.1.2. Coupling of Precipal and Alsoft

As explained in Section 2.6 the coupling of the two models was a relatively simple procedure, as the programs are structured very similarly. It should however be noted that some minor changes to the Alsoft code was necessary (see Appendix B for details). This means that Precipal can not be coupled to a newer version of Alsoft that does not contain these changes. It would however be trivial to implement the necessary changes in a new

version, and the changes would have no effect on Alsofts ability to run separately (i.e uncoupled).

The performance of the coupled model is acceptable, as the performance sensitive part (i.e the solving of the differential equations) is handled by a Fortran code, as described in the previous section. Some combinations of input parameters (use of the phenomenological precipitation model especially) can lead to long run times (more than 10 minutes). This time can however be greatly reduced by adjusting the *rtol* parameter in the integrator (has to be changed in the Alprec code) which sets the maximum error accepted by the integrator (odeint). Changing this parameter to higher values can reduce the run time of the simulations by orders of magnitudes (i.e from over 10 minutes to a few seconds), without having any noticeable effect on the result. This also fixes some out of memory errors which can occur during long simulations. The default values used by the integrator is 1.49012×10^{-8}, while the default value used in Alprec is 1.49012×10^{-5}. For the simulations done in this thesis this value have proved to give satisfactory results in a reasonable time frame.

4.2. Precipal

In this section discussion regarding uncoupled Precipal simulations are presented.

4.2.1. Sensitivity test

The most uncertain parameters in the sensitivity test performed in Section 3.3 that also have a major effect on the precipitation is the equilibrium solubility prefactor, C_s, and the interface energy modifier, ξ. The former should in principle be well defined from thermodynamics, however, the thesis of Lok left some uncertainties about the principal value of this parameter and it is therefor included in the sensitivity analysis. The concentration inside the dispersoids and constituents also have a large effect on the precipitation, however these parameters have a clearly defined theoretical value (the stoichiometric concentrations), so their values are mostly predetermined. The last parameters investigated in the sensitivity test, the initial number of dispersoids (N_{d0}) had only limited effect on the precipitation.

From the sensitivity analysis it can be seen that tuning of the equilibrium solubility prefactor, C_s and the interface energy modifier, ϵ, affect the volume fraction and number of dispersoids, and the solid solution concentration, in almost the same way, with the exception of the equilibrium solubility (i.e the final solid solution concentration), which is only dependent on C_s. This means that C_s can be used to fit the equilibrium solubility to experimental data, while ξ can be used to adjust the volume density and number of dispersoids. It is reasonable to fit both these values to experimental data, as they have no well defined theoretical, and/or easily available, value. A problem that arises with this approach is that the number density relative to the volume fraction of dispersoids (and due to the relationship in Eq. A.2 also the radius) can not be changed by these parameters. One way to change the relationship is to adjust the Mn concentration inside the dispersoids, C_d, as adjusting this will change the volume fraction of dispersoids, while not affecting the number density. Using this parameter as a fitting parameter however is problematic, as it has a very easily calculated theoretical value, i.e the stoichiometric

concentration. The same can be said about the Mn concentration inside the constituents, C_s, as changing this value effects the number density and volume fraction of dispersoids, as well as the initial solid solution concentration, but also this parameter should be set to the stoichiometric value.

The initial solid solution concentration is decided by the number density and size of the constituent particles, and the Mn concentration inside the constituents (in addition to the nominal alloy concentration). The solid solution concentration is relatively easy to measure, e.g by thermoelectric power (TEP) or hardness tests[6, 7], or calculated based on thermodynamic data (e.g by the use of the MTDATA software tool)[6]. This can not, however, say anything about the relation between the size, number density and volume density of the constituents. To obtain information about this relationship optical microscopy (mainly for constituents) or scanning electron microscopy (SEM) can be used.

4.2.2. Comparison of Precipal with simulations by Lok

Physical precipitation model

As already mentioned in Section 3.4 the precipitation model in Precipal is based on the model presented in the PhD thesis of Lok[6], and due to this it was expected that Precipal would be able to reproduce the results presented in his thesis. As the results presented here has shown, this was not the case for the physical precipitation model. More simulations than presented in this thesis was performed in order to try to replicate his results, with different interpretations of the input parameters presented in his thesis, however, none of this simulations produced results which corresponded with his results. It is currently unknown if the problem lies in the input parameters used, or in the implementation of the precipitation model. It should be noted that Lok's results also failed to reproduce his experimental data with the physical model, so it can not be said that his model is more correct than the current implementation of Precipal.

The physical site-saturation simulations is better in reproducing Lok's results. This could imply that the discrepancy between the models are related to the nucleation calculations, however this improved accordance could also simply be due to the loss of one degree of freedom, i.e the number of dispersoids is now set as a constant input parameter.

It is hard to pinpoint the source of the different results based on the performed simulations. Even though Precipal was not able to reproduce the simulation results presented by Lok in his thesis, the rest of the work in this thesis was carried out with confidence in the parameter choices made in this work, and correspondingly the simulation results produced by Precipal, as it produced the same results as the old Fortran implementation.

It is interesting that for the undeformed material (Fig. 3.7) the current Precipal simulations give precipitation later than Lok's results, while in the deformed case (Fig. 3.8) Precipal starts precipitation before the corresponding simulations made by Lok. This means that there is a difference in how the variation in precipitation conditions between the deformed and undeformed is handled by the two implementations. This observation is not valid for the site-saturation cases, as the Precipal precipitation curves in this case match the results of Lok.

Phenomenological precipitation model

As shown in Section 3.4.2 the phenomenological model in Precipal reproduces Lok's phenomenological simulations. However, as already mentioned the fitting parameters used in Precipal are numerically different from the values used by Lok, mainly because Precipal uses at %, while Lok in his thesis states all concentrations in wt %. The values of the fitting parameters used in Precipal were obtained by trial and error. Because of this there is no clear correspondence with Lok's fitting parameters except that both Precipal and Lok produce the same results with their respective set of fitting parameters.

The phenomenological model is able to reproduce the experimental data at a given temperature. This is a clear improvement compared with the physical model which failed to reproduce experimental data at any temperature. Especially the evolution of the solid solution concentration is well described by the phenomenological model, while in the physical model the concentration drops too rapidly. At temperatures other than the fitting temperature, however, also the phenomenological model fails to reproduce the experimental data in a satisfactory manner. The usefulness of the phenomenological model is because of this, questionable at best, as it can not be used to predict the effect different temperatures will have on the precipitation course. It is however useful for simulating the precipitation course during coupling with Alsoft, as it does produce realistic results at a given temperature, and can thus be used to test the effects of a realistic change in the solid solution concentration and the number and size of the dispersed particles during recrystallization.

4.3. Coupling of Precipal and Alsoft

In this section discussions regarding coupled Precipal and Alsoft simulations are presented.

Input parameters in the Alsoft model

The input parameters used by Alsoft do not completely coincide with the material used in the experimental data from Lok (as explained in Section 3.5), but any discrepancies due to this should be minimal since the materials are almost identical, and the fitting done to the mobility and grain size, as described in Section 3.5.1 should help to minimize this. It is therefore assumed that the input parameters used in Alsoft should be suitable to simulate the material.

Recrystallization kinetics

When the recrystallization curve from uncoupled Alsoft simulations were fitted to experimental data at 450 °C by tuning the mobility, the recrystallization curve at 425°C was also reproduced satisfactory by Alsoft (by only changing the temperature), as was shown in Figure 3.12a. At other (lower) temperatures the incubation time before onset of recrystallization was greatly underestimated by Alsoft (i.e recrystallization occurred to early). As can be seen in Figure 3.12a this is also the two temperatures where experimentally recrystallization occurs before the onset of precipitation, and since Alsoft do not simulate precipitation (i.e the Zener-drag and solid solution concentration is constant, and the same at all temperatures) it is not surprising that the experimental recrystallization

behavior that undergo concurrent precipitation experience a stronger temperature dependence. This is the same as reported by Wang[11], where he states that Alsoft is able to produce satisfactory softening behavior for conditions where there are no concurrent precipitation of dispersoids.

It was believed that coupling of Alsoft with the precipitation model would improve its ability to reproduce the experimental curves at lower temperatures, but as shown in Figure 3.12b and 3.12c this was not the case. The coupling had very limited effect on the recrystallization kinetics (except when recrystallization was halted completely). The change in the Zener-drag and solid solution concentration in Alsoft due to the coupling was not enough to have a meaningful impact on the recrystallization kinetics.

Underestimation of dispersoid effect in Alsoft was also reported by Wang et.al[11]. In this work they managed to use Alsoft to successfully reproduce softening curves when the particle effects were small, but also here the model failed to provide reasonable predictions when particles were experimentally shown to have a large impact on the recrystallization course.

The cause of the underestimated effects of precipitation on the recrystallization behavior is believed to be due to an underestimation of the effects the Zener-drag has on nucleation. The assumption of site-saturation recrystallization nucleation is problematic in conditions of concurrent precipitation, where the Zener-drag is low at t=0 (when nucleation occurs during site-saturation). With this assumption only the contribution from large primary particles (constituents) are included. i.e not the effects of the much larger Zener-drag from the later concurrent precipitation of the smaller precipitates.

This problem related to site-saturation nucleation of recrystallization can also be noticed from the simulated grain sizes compared with the experimental ones, as shown in Figure 3.13. Here it can be seen that there is a dramatic increase in the experimental grain size when the temperature is decreased from 450 to 405 °C, while the simulated grain size is unchanged (when 100 % of the material is recrystallized). This discrepancy between the simulated and experimental grain sizes can be attributed to the inherent problem with site-saturation nucleation, in which the effects of concurrent precipitation on nucleation is neglected, i.e suppressed nucleation of recrystallization due to pinning of the sub-grain structure (analog to the pinning effect on moving grain boundaries explained in Sec. 2.3.2) implying a strong reduced density of nucleation sites. The effect is particularly pronounced for conditions with considerable (concurrent) precipitation before onset of recrystallization.

Simulation with an extra artificial Zener-drag during nucleation was performed in order to identify how much additional Zener-drag was needed to reproduce the experimental recrystallization curves. It was found that an extra Zener-drag of 230 kPa during nucleation was sufficient to reproduce the experimental recrystallization curves at 405 °C (Fig. 3.17). It should be noted that the Zener-drag had to be set to zero (or a low value) after nucleation (i.e when recrystallization starts), in order to get full recrystallization consistent with experiments. The originally calculated Zener-drag during nucleation at this temperature was only 16 kPa, which means that the Zener-drag during nucleation required to reproduce the experimental results was more than 16 times larger. This clearly shows that the current recrystallization nucleation model assuming site saturation is inadequate for simulating the effects of precipitation on nucleation. Moreover the fact that the Zener-drag has to be ”turned off” in conditions of significant precipitation to avoid a complete

stop in the recrystallization process indicates that the Zener-drag effects during recrystallization, once started, is much less than a classical Zener-drag (Eq. 2.2) provides. This latter observation is consistent with the findings of Wang[11] and unpublished theoretical calculations by Rollett[27].

The simulated grain size with this extra Zener drag during nucleation is about 2 mm (diameter) (Fig. 3.16). This is significantly larger than the experimental size of 0.5 mm (Fig. 3.13). It is noted however that the grain size is critically dependent on the value of the initial Zener-drag (in this high range regime), and moderate changes can give significant changes in the grain size.

5. Conclusion

The reimplementation of Precipal in Python was successful, as the new implementation is able to fully reproduce the results from the old implementation. In accordance with Lok, Precipal includes two approaches to calculate the precipitation evolution, i.e a physically based model and a phenomenological approach. However, the physical model with apparently the ”same” input parameters was not able to reproduce the corresponding simulation results of Lok. The phenomenological model on the other hand provided consistent results with Lok, although with different fitting parameters. The phenomenological model's predictive power at different annealing temperatures was however proven to be limited, but it provides a realistic precipitation course at a given temperature that can be used when coupled with Alsoft.

The coupling of Alsoft and Precipal through their external parameters was accomplished with only minor changes to the Alsoft code. The coupling did not have a significant impact on the simulated recrystallization behavior. The reason for this is believed to be found in the nucleation model used in Alsoft, i.e the inherent shortcoming of the site-saturation model, which fails to account for the effect of concurrent precipitation on nucleation of recrystallization.

Future work that needs to be done includes validation of the precipitation model against more experimental data, and to couple the precipitation model with a time dependent recrystallization model, i.e a model which is capable of including the effect of (concurrent) precipitation on nucleation of recrystallization. This latter aspect seems to be the key to explain the recrystallization behavior in conditions of concurrent precipitation.

Bibliography

[1] K. Marthinsen, T. Furu, E. Nes, and N. Ryum. "Modelling of recrystallization". In: *Proc. of Fall Meeting of the Minerals, Metals and Materials Society*. Ed. by M.P. Anderson and A.D. Rollett. Minerals, Metals, and Materials Society, 1990, p. 87. URL: http://books.google.no/books?id=iWowAAAAIAAJ.

[2] T. Furu, K. Marthinsen, and E. Nes. "Modeling recrystallization". In: *Mater. Sci. Technol.* 6.11 (1990), pp. 1093–102.

[3] H. E. Vatne, T. Furu, R. Orsund, and E. Nes. "Modeling recrystallization after hot deformation of aluminum". In: *Acta Mater.* 44.11 (1996), pp. 4463–4473. DOI: 10.1016/1359-6454(96)00078-x.

[4] J. Friis. "Equations used in the Fortran 77 version of PrecipAl". Revision 13. November 2006.

[5] J. Friis. "New formulations of PrecipAl". Revision 23. January 2013.

[6] Z.J. Lok. "Microchemistry in aluminium sheet production". PhD thesis. 2005. URL: http://resolver.tudelft.nl/uuid:38aa1c82-f543-42e9-b55c-f0a1b51c0214.

[7] Stian Tangen. "Deformation and annealing behavior of commercial non-heat treatable aluminium alloys". Doctoral Thesis. Trondheim, 2004.

[8] G. Sande. "Softening Behaviour of Selected Commercially Pure Aluminium Model Alloys". Master thesis. 2012. URL: http://urn.kb.se/resolve?urn=urn:nbn:no:ntnu:diva-18897.

[9] B. Verlinden, J. Driver, I. Samajdar, and R.D. Doherty. *Thermo-Mechanical Processing of Metallic Materials*. Elsevier Science, 2007. ISBN: 9780080544489. URL: http://books.google.no/books?id=VE20YVDTBZUC.

[10] F. J. Humphreys and M. Hatherly. *Recrystallization and related annealing phenomena*. 2nd ed. England: Elsevier, 2004. ISBN: 9780080441641. URL: http://books.google.no/books?id=52Gloa7HxGsC.

[11] Ning Wang. "Softening behaviour o fAl-Mn-Fe-Si alloys during isothermal annealing". PhD thesis. NTNU, 2013. URL: http://urn.kb.se/resolve?urn=urn:nbn:no:ntnu:diva-23706.

[12] O. Engler, L. Loechte, and J. Hirsch. "Through-process simulation of texture and properties during the thermomechanical processing of aluminum sheets". In: *Acta Mater.* 55.16 (2007), pp. 5449–5463. DOI: 10.1016/j.actamat.2007.06.010.

[13] H Cama, R Ricks, R Hamerton, and J Humphreys. *aluMATTER*. Web Page. 2014. URL: http://aluminium.matter.org.uk/content/html/eng/default.asp?catid=68&pageid=803396170.

[14] K. Sjølstad. "Deformation and Softening behaviour of commercial AlMn-alloys : Experiments and Modelling". PhD thesis. 2003. URL: http://urn.kb.se/resolve?urn=urn:nbn:no:ntnu:diva-143.

[15] J Iversen. "Modellering av gjenvinning og rekrystallisasjon i aluminium med Alsoft". Project thesis at NTNU. 2013.

[16] K. Marthinsen, J. Friis, B. Holmedal, I. Skauvik, and T. Furu. "Modelling the recrystallization behaviour during industrial processing of aluminium alloys". In: *Mater. Sci. Forum* 715-716.Recrystallization and Grain Growth IV (2012), pp. 543–548. DOI: 10.4028/www.scientific.net/MSF.715-716.543.

[17] J. Fris, O. Engler, and K. Marthinsen. "Equations used in the time-dependent version of Alsoft". Revisjon 7. November 2013.

[18] H. S. Zurob, Y. Brechet, and J. Dunlop. "Quantitative criterion for recrystallization nucleation in single-phase alloys: Prediction of critical strains and incubation times". In: *Acta Mater.* 54.15 (2006), pp. 3983–3990. DOI: 10.1016/j.actamat.2006.04.028.

[19] J. W. C. Dunlop, Y. J. M. Brechet, L. Legras, and H. S. Zurob. "Modeling isothermal and non-isothermal recrystallisation kinetics: Application to Zircaloy-4". In: *J. Nucl. Mater.* 366.1-2 (2007), pp. 178–186. DOI: 10.1016/j.jnucmat.2006.12.074.

[20] *Wikipedia*. Web Page. 2014. URL: http://en.wikipedia.org/wiki/File:Avrami_transformation_plot.svg.

[21] K. T. Kashyap and R. George. "Mechanism of cube grain nucleation during recrystallization of deformed commercial purity aluminum". In: *Bull. Mater. Sci.* 29.2 (2006), pp. 197–200. DOI: 10.1007/BF02704616.

[22] Masakazu Kobayashi, Yoshimasa Takayama, and Hajime Kato. "Preferential growth of cube-oriented grains in partially annealed and additionally rolled aluminum foils for capacitors". In: *Mater Trans* 45.12 (2004), pp. 3247–3255. URL: https://www.jim.or.jp/journal/e/45/12/3247.html.

[23] J. A Sæter, B. Forbord, H. E. Vatne, and E. Nes. *Modelling recovery and recrystallization, applied to back-annealing of aluminium sheet alloys*. Vol. 1. Procedings of 6th International Conference on Aluminium Alloys. Toyohashi, Japan: the Japan Institute of Light Metals, 1998, pp. 113–126.

[24] N. Wang, K. Huang, and K. Marthinsen. "Modelling recovery and recrystallization behavior of cold-rolled Al-Mn-Fe-Si-alloys with different micro-chemistries". NTNU, Trondheim, Norge, 2013.

[25] P. Peterson. "F2PY: a tool for connecting Fortran and Python programs". In: *International Journal of Computational Science and Engineering* 4.4 (2009), pp. 296–305. DOI: 10.1504/IJCSE.2009.029165.

[26] P Langtangen H and X. Cai. "On the Efficiency of Python for High-Performance Computing: A Case Study Involving Stencil Updates for Partial Differential Equations". In: *Modeling, Simulation and Optimization of Complex Processes*. Ed. by H. G. Bock, E. Kostina, H. Phu, and R. Rannacher. Springer Berlin Heidelberg, 2008. Chap. 23, pp. 337–357. ISBN: 978-3-540-79408-0. DOI: 10.1007/978-3-540-79409-7_23.

[27] A. D. Rollett. Personal Communication. 2014.

A. Derivation of Selected Equations

A.1. Volume fraction and radius of particles

The radius and volume fraction of particles are, owing to geometry reasons, related by the following equation[4]:

$$f = \frac{4}{3}\pi r^3 sN \tag{A.1}$$

Where f is the volume fraction of particles, r is the particle radius, N is the number of dispersoids and s is a factor accounting for the width of the particle size distribution.

The equation can be rearranged to give an expression for the particle radius:

$$r = \left(\frac{3f}{4\pi s_c N_c}\right)^{1/3} \tag{A.2}$$

A.1.1. Constituents

For constituents the subscript c is used, giving the following equations for volume fraction and particle radius:

$$f_c = \frac{4}{3}\pi r_c^3 S_c N_c \tag{A.3}$$

$$r_c = \left(\frac{3f_c}{4\pi s_c N_c}\right)^{1/3} \tag{A.4}$$

Volume Fraction:

The number of constituents is assumed to be constant, and the time derivative of the volume fraction can thus be expressed by:

$$\frac{df_c}{dt} = \frac{4}{3}\pi S_c N_c r_c^2 \frac{dr_c}{dt} = \frac{4}{3}\pi S_c N_c r_c^2 V_c \tag{A.5}$$

here $V_c = \frac{dr_c}{dt}$.

Radius:

By differentiation of equation A.4 the time derivative of the particle radius is:

$$\frac{dr_c}{dt} = \frac{1}{3\left(\frac{3f_c}{4\pi s_c N_c}\right)^{2/3}} \frac{3}{4\pi s_c N_c} \frac{df_c}{dt} \tag{A.6}$$

Rearranging and insertion of Eq. A.3 and A.5 gives:

$$\frac{dr_c}{dt} = 3\left(\frac{4\pi s_c N_c}{3\frac{4}{3}\pi r_c^3 S_c N_c}\right)^{2/3} \frac{3}{4\pi s_c N_c}\frac{4}{3}\pi S_c N_c r_c^2 V_c \tag{A.7}$$

where $V_c = \frac{dr_c}{dt}$ is the growth rate of the dispersoids.
This equation can be reduced to:

$$\frac{dr_c}{dt} = V_c \tag{A.8}$$

A.1.2. Dispersoids

For dispersoids the subscript d is used, giving the following equations for volume fraction and radius:

$$f_d = \frac{4}{3}\pi r_d^3 S_d N_d \tag{A.9}$$

$$r_d = \left(\frac{3 f_d}{4\pi s_d N_d}\right)^{1/3} \tag{A.10}$$

In contrast to the number constituents, the number of dispersoids is not assumed to be constant. This gives more complex expressions for the time derivatives.

Volume Fraction:

By differentiation of Eq. A.9 the time derivative for the volume fraction of dispersoids can be expressed by:

$$\frac{df_d}{dt} = \frac{4}{3}\pi s_d\left[3r_d^2\frac{dr_d}{dt}N_d + r_d^3\frac{dN_d}{dt}\right] = \frac{4}{3}\pi s_d\left[3r_d^2 V_d N_d + r_d^3 J_d\right] \tag{A.11}$$

where $J_d = \frac{dN_d}{dt}$ and $V_d = \frac{dr_d}{dt}$.

Radius:

Differentiation of Eq. A.10 gives the following expression for the time derivative of the dispersoid radius:

$$\frac{dr_d}{dt} = \frac{1}{3\left(\frac{3f_d}{4\pi s_d N_d}\right)^{2/3}}\frac{3}{4\pi s_d}\left[\frac{df_d}{dt}\frac{1}{N_d} - f_d\frac{dN_d}{dt}\frac{1}{N_d^2}\right] \tag{A.12}$$

Combination with Eq. A.9 and A.10 gives:

$$\frac{dr_d}{dt} = \frac{1}{3\left(\frac{3\frac{4}{3}\pi r_d^3 S_d N_d}{4\pi s_d N_d}\right)^{2/3}}\frac{3}{4\pi s_d}\left[\frac{4}{3}\pi s_d\left[3r_d^2 V_d N_d + r_d^3 J_d\right]\frac{1}{N_d} - \frac{4}{3}\pi r_d^3 S_d N_d\frac{dN_d}{dt}\frac{1}{N_d^2}\right] \tag{A.13}$$

Which can be reduced to:

$$\frac{dr_d}{dt} = \frac{1}{3r_d^2}\left[\left[3r_d^2 V_d N_d + r_d^3 J_d\right]\frac{1}{N_d} - r_d^3 J_d \frac{1}{N_d}\right] \tag{A.14}$$

This expression can be further reduced to give the final expression for the time derivative for the dispersoid radius:

$$\frac{dr_d}{dt} = V_d \tag{A.15}$$

B. Changes to the Alsoft code

In this section all changes done to the Alsoft source code are presented and explained. First the changes related to the coupling are presented, followed by an explanation of the new features introduced.

B.1. Changes related to the coupling

The input parameter *PZ_from_chemistry*, which specifies where the Zener-drag are read from, was given a third option, "2", which specifies that the values should be provided by the coupling with Precipal. This change was necessary even though the reference to the function for getting external parameters are handled externally during the coupling since this originally external parameter is also accessed by *get_constpar()*, which calculates all the constant parameters at the start of execution.

When the input parameter *PZ_from_chemistry* is set to "2" the initial value for PZ used during calculation of the constant parameters are provided by the shell function *GetPz0FromPrecipal()*. This function has no functionality in Alsoft, the reference to the function is meant to be taken over by a Alprec function, as explained in Section 2.6 in the main text.

B.2. New features

The possibility to set the Zener-drag to zero after a certain fraction recrystallized was introduced. This new featured is controlled by two new input parameters; *PZ_only_during_rec* which enables (=1) or disables (=0) this feature, and *recryst_start* which specifies the fraction recrystallized when the Zener-drag should be set to zero (number between 0 and 1). This feature is implemented by a simple test in *fun()* which sets the Zener-drag to zero if the conditions specified by the input parameters are met.

This feature was introduced in order to simulate the effect of a high Zener-drag during nucleation, but with subsequent recrystallization and grain growth unhindered by the Zener-drag. This is motivated by the experimental work by Wang[11], and also by theoretical calculations by others[27]

A minor feature that was introduced was the possibility to down sample the output before writing it to file. This change was necessary as some combinations of input parameters lead to long integration times and an extremely high number of time steps Up to several hundred thousand time steps, resulting in output files larger than 150 Mb. This was implemented as a basic down sampling with no interpolation. This new feature is controlled through an optional keyword parameter, *maxSamples*, in the *write_results()* function which specifies the maximum number of time steps to be written to file.

C. Input Parameters

C.1. Precipal

Value	Python	Symbol	Desription
0	alsoft	N/A	Mode bit flag: 0=stand-alone 1=coupled with alsoft
1	ext_t	N/A	Mode bit flag: 0=external time 1=extra timesteps (between max and min in trt file)
0	SS	N/A	Mode bit flag: 0=normal nucleation 1=site saturation
0	t_inc	N/A	Incubation time for precipitation (used if SS=1). S
0	mode	N/A	Mode bit flag: 0=physical model 1=phenomenological model
1	evEq	N/A	Mode bit flag: 0 = old evolution eq. (f_d, f_c) 1 = new evolution eq.(r_d, r_c)
0	N_d0	$N_d(0)$	Initial dispersoid density. 1/mˆ3 (not used if SS=1)
0	f_d0	$f_d(0)$	Initial dispersoid volume fraction (Used if evEq=0)
0.0404296	f_c0	$f_c(0)$	Initial constituents volume fraction (Used if evEq=0)
0	r_d0	$r_d(0)$	Initial dispersoid radius. M (Used if evEq=1)
1.12E-006	r_c0	$r_c(0)$	Initial constituents radius. M (Used if evEq=1)
4.096E-010	a0	a_0	Lattice parameter of matrix (assuming fcc). M
6.87E+015	N_c	N_c	Number density of const. 1/mˆ3

9.68E-006	Vm_d	V_m^d	Molar volume of disp. M^3/mol
0.05	Zeldovic	Z	Zeldovic factor
4.0496E-010	t_SGB	t_{SGB}	Eff. Subgrain boundary thickness. M
0.324	gamma_d	γ_d	Disp.-matrix interface energy. J/m^2
1.66026E-029	eta	η	Atomic volume of matrix (= a0^3/4 for fcc). m^3
0.6	xi	ξ	Interface energy modifier (0 < xi < 1)
1	s_d	s_d	Factor accounting for the width of the constituent size distribution
1	s_c	s_c	Factor accounting for the width of the dispersoid size distribution

C.2. Alsoft

Value	Python	Symbol	Desription
1	site_saturation	N/A	Nucleation type: 0 = time dependent 1 = site saturation
0	Gamma_distr	N/A	Subgrainsize distribution: 0=log-normal 1=gamma
0	init_recovery	N/A	Submodel for initial value of rho_i0 and delta0: 0=from input 1=from flow stress 2=from strain rate
2	Css_from_chemistry	N/A	Where to read Css from: (No effect when coupled) 0=treatment table 1=chemistry 2=Precipal
2	PZ_from_chemistry	N/A	Where to read PZ from 0=treatment table 1=chemistry 2=Precipal (coupling)
0	PZ_only_during_rec	N/A	Zener-drag only during nucleation: 0=normal Zener-drag 1=PZ only during nucleation
0	recryst_start	N/A	Cut-of fraction for recrystallization start
$1.98E+13$	rho_i0	ρ_0	Initial dislocation density (#/m^2)
1E-006	delta0	δ_0	Initial subgrain size (m)
0	Xext0	$X_{ext,0}$	Initial extended volume fraction
0	Sext0	$S_{ext,0}$	Initial extended surface fraction (m^-1)

6E-007	Dext0	$D_{ext,0}$	Initial extended grain size (m)
1	NGB0	$N_{GB,0}$	Initial number density of nucleation sites (not used for site-saturation)
1	NCube0	$N_{Cube,0}$	Initial number density of nucleation sites (mˆ-3) (not used for site-saturation)
1	NPSN0	$N_{PSN,0}$	Initial number density of nucleation sites (mˆ-3) (not used for site-saturation)
0.00393	Css_0	C_{ss}	Constant in expr. For effective solute content (at. fraction)
1	C_PZ	C_{PZ}	Prefactor for Zener drag
0.5	FTh		Final sheet thickness (mm), unused
3	strain0	ϵ	True strain
50	strainRate0		Strain rate (1/s)
20	T_def	T_{def}	Temperature during deformation (C)
200	Rp02_0	R_{p02}	Initial flow stress (MPa)
53	R_FLP	R_{FLP}	Friction stress (MPa)
0.25	f_rho	f_ρ	Constant in alternative expr. For initial rho_i and delta
$8.00E+04$	B_rho	B_ρ	Constant in evolution eq. for dislocation density
0.5	w_rho	w_ρ	Constant in evolution eq. for dislocation density
2	B_delta	B_δ	Constant in evolution eq. For subgrain size
5	w_delta	w_δ	Constant in evolution eq. for subgrain size
2.67E+017	N0	N_0	Constant in particle size distribution (1/m)
$3.14E+06$	L	L	Constant in particle size distribution (1/m)
$1.20E+05$	M0	M_0	Prefactor for mobility (mˆ4/s)
0.04	As	A_s	Constant in initial subgrain size
0.03	Bs	B_s	Constant in initial subgrain size
2	C_1	C_1	Constant in initial dislocation density
0.0001	D0	D_0	Initial (as-cast) grain size (m)
0.6667	e_delta	e_δ	Constant in evolution eq. for subgrain size
0.6667	e_rho	e_ρ	Constant in evolution eq. for dislocation density
0.3	alpha1	α_1	Constant in strength model
2.5	alpha2	α_2	Constant in strength model
3	Mtaylor	M_{taylor}	Taylor factor
2.86E-010	b	b	Burgers vector (m)
$1.00E+13$	v_D	ν_D	Debye frequency (1/s)
0.3	gamma_GB	γ_{GB}	Grain boundary energy (J/mˆ2)
1.2	CPE	C_{PE}	Constant in expr. For density of PSN sites
0.0247	C_PSN	C_{PSN}	Prefactor for density of PSN sites
0.005069	C_GB	C_{GB}	Constant in expr. For density of PSN sites (mˆ3)
2.5	alpha	α	Constant in expr. For density of GB nucleation sites

			nstant in expr. for density of cube nucleation sites
4	theta	θ	Geometric constant in driving pressure
15	theta_c	θ_c	for recrystallisation
0.33	nu	ν	Missorientation (Deg.)
0.04	R_c0	R_{c0}	Constant for missorientation (Deg.)
85.517	C_Cube	C_{Cube}	Poisson number
1.3	fCube	f_{cube}	Initial volume fraction of cube grains
2.6	R_cA	R_{cA}	Scale factor for mean cube grain size
1	R_cB	R_{cB}	Constant in expr. for volume fraction cube grains
0.3	R_cC	R_{cC}	Constant in expr. for volume fraction cube grains
-2	R_cD	R_{cD}	Constant in expr. for volume fraction cube grains
0.1	R_cE	R_{cE}	Constant in expr. for volume fraction cube grains
-1.4	R_cF	R_{cF}	Constant in expr. for volume fraction cube grains
-1.8	R_cG	R_{cG}	Constant in expr. for volume fraction cube grains
0.04	R_sA	R_{sA}	Constant in expr. for volume fraction cube grains
0.173	R_sB	R_{sB}	Constant in expr. for fraction S deformation texture
2	R_sC	R_{sC}	Constant in expr. for fraction S deformation texture
$2.00E+05$	U_a	U_a	Constant in expr. for fraction S deformation texture
$1.80E+05$	U_aGB	$U_{a,GB}$	Eff. activation energy for solute diffusion (J/mol)
$2.00E+05$	U_aCube	$U_{a,Cube}$	Eff. activation energy cube subgrains (J/mol)
$2.00E+05$	U_aPSN	$U_{a,PSN}$	Eff. activation energy GB subgrains (J/mol)
$2.00E+05$	U_rex	U_{rex}	Eff. activation energy PSN subgrains (J/mol)
$2.00E+05$	U_GB	U_{GB}	Activation energy for recrystallisation (J/mol)
$1.60E+05$	U_ZH	U_{ZH}	Activation energy for grain boundary (J/mol), unused
0.04	f0	f_0	Activation energy for Zener-Hollomon par. (J/mol)
3	kaa	k_{aa}	Fraction of PSN-nuclei being cube, unused
$2.65E+10$	G0	G_0	Constant in expr. for rho_t
0	G1	G_1	Prefactor in expr. for shear modulus (Pa)
1	nu0_Cube	$\nu_{Cube,0}$	Exp. Factor in expr. For shear modulus (K^-1)
1	nu0_PSN	$\nu_{PSN,0}$	Prefactor in expr. for nucleation frequency (s^-1)
1	nu0_GB	$\nu_{GB,0}$	Prefactor in expr. for nucleation frequency (s^-1)
$9.00E+04$	Qnu0_Cube	$Q\nu_{Cube,0}$	Prefactor in expr. for nucleation frequency (s^-1)
$9.00E+04$	Qnu0_PSN	$Q\nu_{Cube,0}$	Activation energy in expr. For nuc. Frequency (J/mol)
$9.00E+04$	Qnu0_PSN	$Q\nu_{Cube,0}$	Activation energy in expr. For nuc. Frequency (J/mol)
1	Crho	C_ρ	Activation energy in expr. For nuc. Frequency (J/mol)
1	Cdelta	C_δ	Constant for including Zener drag force on dislocation annihilation rate. Should be one.
0.7	K_GB0	$K_{GB,0}$	Constant for including Zener drag in subgrain growth. Should be one.
1	K_Cube0	$K_{Cube,0}$	Factor in the initial grain boundary subgrain size
1	K_PSN0	$K_{PSN,0}$	Factor in the initial cube subgrain size

0.4545	sGB	S_{GB}	Factor in the initial PSN subgrain size
0.4545	sCube	S_{Cube}	Shape parameter for size distr. GB subgrains
0.4545	sPSN	S_{PSN}	Shape parameter for size distr. Cube subgrains
			Shape parameter for size distr. PSN subgrains

C.3. Treatment table

time(s)	**T(C)**	**X**	**delta(μm)**	**Css(at. Frac)**	**PZ(Pa)**
0	405	1	2	0.004586	0
60000	405	1	2	0.004586	0

This is the treatment table used in the simulations with undeformed material. Note that fraction recrystallized, X, the subrain size, delta, the solid solution concentration, Css, and the Zener-drag, PZ, is not used during the coupled simulations. X and delta is only used during uncoupled Precipal simulations, while Css and PZ is only used during uncoupled Alsoft simulations.

C.4. Element table

	Mn	**Fe**	**Si**	**Al**
C0(wt%)	1.11	0.51	0.06	98.32
M(g/mol)	54.938	55.847	28.0855	26.98154
D0_L(m^2/s)	0.0104	0	0	0
Qd_L(J/mol)	210900	195000	140000	0
D0_SGB(m^2/s)	0.0104	0	0	0
Qd_SGB(J/mol)	126500	0	0	0
Cs(atFrac)	38.21	0	0	0
Qc(J/mol)	71500	0	0	0
Cd_ppt(at%)	18.75	0	6.25	0
Cc_ppt(at%)	14.286	0	0	0